

TIME DOMAIN TERAHERTZ SPECTROSCOPY: CONSTRUCTION OF THE  
SETUP AND APPLICATION IN ANALYSIS OF ACTIVE PHARMACEUTICAL  
INGREDIENTS

A THESIS SUBMITTED TO  
THE GRADUATE SCHOOL OF NATURAL AND APPLIED SCIENCES  
OF  
MIDDLE EAST TECHNICAL UNIVERSITY

BY

YUSUF SAMET AYTEKİN

IN PARTIAL FULFILLMENT OF THE REQUIREMENTS  
FOR  
THE DEGREE OF MASTER OF SCIENCE  
IN  
CHEMISTRY

AUGUST 2016



Approval of the thesis:

**TIME DOMAIN TERAHERTZ SPECTROSCOPY: CONSTRUCTION OF  
THE SETUP AND APPLICATION IN ANALYSIS OF ACTIVE  
PHARMACEUTICAL INGREDIENTS**

submitted by **YUSUF SAMET AYTEKİN** in partial fulfillment of the requirements  
for the degree of **Master of Science in Chemistry Department, Middle East  
Technical University** by,

Prof. Dr. Gülbin Dural Ünver  
Dean, Graduate School of **Natural and Applied Sciences**... \_\_\_\_\_

Prof. Dr. Cihangir Tanyeli  
Head of Department, **Chemistry** ..... \_\_\_\_\_

Assoc. Prof. Dr. Okan Esentürk  
Supervisor, **Chemistry Dept., METU** ..... \_\_\_\_\_

**Examining Committee Members:**

Assoc. Prof. Dr. Gülay Ertaş  
Chemistry Dept., METU ..... \_\_\_\_\_

Assoc. Prof. Dr. Okan Esentürk  
Chemistry Dept., METU ..... \_\_\_\_\_

Assoc. Prof. Dr. Mehmet Fatih Danışman  
Chemistry Dept., METU ..... \_\_\_\_\_

Assoc. Prof. Dr. Hakan Altan  
Physics Dept., METU ..... \_\_\_\_\_

Asst. Prof. Dr. Bülend Ortaç  
UNAM , Bilkent..... \_\_\_\_\_

**Date: 22.08.2016**

**I hereby declare that all information in this document has been obtained and presented in accordance with academic rules and ethical conduct. I also declare that, as required by these rules and conduct, I have fully cited and referenced all material and results that are not original to this work.**

Name, Last Name : Yusuf Samet Aytakin

Signature :

## ABSTRACT

### **TIME DOMAIN TERAHERTZ SPECTROSCOPY: CONSTRUCTION OF THE SETUP AND APPLICATION IN ANALYSIS OF ACTIVE PHARMACEUTICAL INGREDIENTS**

Aytekin, Yusuf Samet

M.S., Department of Chemistry

Supervisor: Assoc. Prof. Dr. Okan Esentürk

August 2016, 84 pages

The purpose of this thesis is to build a homemade Terahertz (THz) Time Domain Spectrometer and analysis of Active Pharmaceutical Ingredients (API) by using the built THz-TDS spectrometer. Several configurations of THz-TDS system were setup and tested in order to optimise experimental parameters. These set-ups can be grouped into two; antenna-antenna and antenna-crystal. In antenna-antenna systems, photoconductive antenna (PCA) and interdigital photoconductive antenna (iPCA) were employed and both were tried for generation and detection of THz field. None of the two set-ups resulted in a good signal-to-noise ratio (SNR) or dynamical range (DR) both in time domain and frequency domain. In antenna-crystal systems, both PCA and iPCA were employed for terahertz generation and 500  $\mu\text{m}$  ZnTe crystal was used for electro-optic sampling. In this case, iPCA-crystal combination gave the best SNR and larger dynamical range. Once the generation and detection types were determined, optimisation studies were carried out to measure optical properties of APIs. A modelocked oscillator Ti:Sapphire laser with central wavelength of 800 nm, repetition rate of 80 MHz, pulse duration of 80 fs and output power of  $\sim 550$  mW was used as the

laser source to generate and detect THz radiation. The final system has 3 THz bandwidth and  $> 10^5$  SNR. Afterwards, several APIs of common drugs were analysed by using both the optimised homemade THz-TDS setup and FT-THz system. The results have shown that each API had a characteristic THz spectrum, that can be used for the identification and characterisation of API.

Keywords: Terahertz, Terahertz Time Domain Spectrometer, Active Pharmaceutical Ingredient Analysis

## ÖZ

### ZAMAN ÇÖZÜMLÜ TERAHERTZ SPEKTROSKOPİ: SİSTEM KURULUMU VE İLAÇ ETKİN MADDE ANALİZİ ÜZERİNE UYGULAMA

Aytekin, Yusuf Samet

Yüksek Lisans, Kimya Bölümü

Tez Yöneticisi: Doç. Dr. Okan Esenturk

Ağustos 2016, 84 sayfa

Bu çalışmanın amacı Zamana Dayalı Terahertz spektrometre kurmak ve bu spektrometre ile ilaç etkin madde analizini yapmaktır. Sistemin olgunlaşma sürecinde çeşitli sistem konfigürasyonları kurulup test edilmiştir. Bu konfigürasyonlar iki gruba ayrılabilir; anten-anten ve anten-kristal sistemleri. Anten-anten sisteminde PCA ve iPCA antenleri hem terahertz ışını üretmek hem de belirlemek için kullanılmıştır. Lakin, bu iki sistem de sinyalin gürültüye oranı bakımından olumlu sonuçlar vermemiştir. Anten-kristal sisteminde ise PCA ve iPCA antenlerinin ikisi de terahertz ışını üretiminde kullanılırken terahertz belirlemede ise elektro-optik belirleme tekniği için 500 µm ZnTe kristali kullanılmıştır. Sonuç olarak iPCA-kristal kombinasyonu en iyi sinyal-gürültü oranı ve daha geniş çalışma aralığı vermiştir. Terahertz üretme ve belirleme teknikleri saptandıktan sonra sistem optimizasyonu için adımlar atılmıştır. Sistemin kalbini merkezi dalga boyu 800 nm, atım frekansı 80 MHz, atım süresi 80 fs ve çıkış gücü yaklaşık 550 mW olan kip kilitli Ti:Safir lazer teşkil etmektedir. Bu lazer THz üretimi ve belirlenmesi için kullanılmaktadır. Sistemin optimum hali 3 THz bant genişliği ve  $> 10^5$  SNR oranına sahiptir. Sistem optimizasyonu gerçekleştirildikten sonra ilaç etkin maddeleri (İEM) hem kurulan THz sistemi hem de FT-THz teknikleri kullanılarak analiz edilmiştir. Elde edilen İEM

spektrumları her İEM için özgün THz spektrumları vermiştir ve, bu, THz tekniğinin İEM tayini ve tanımlamaları bakımlarından kullanışlı olduğuna işaret etmektedir.

Anahtar kelimeler: Terahertz, Zamana Dayalı Terahertz Spektrometre, İlaç Etkin Madde Analizi

*Сани, саби; зкультура еиқәхарц еснагь иазықәҗаз, иазықәҗоу,  
егьи назаза иазықәҗаша Нхыӡ Кавказтә ауааи ирызкуп...*

## ACKNOWLEDGEMENTS

I would like to express my sincere gratitude to my supervisor Assoc. Prof. Dr. Okan Esentürk for his kind support and patience during my studies. I appreciate his encouraging supervision throughout my studies.

I would like to thank Assoc. Prof. Dr. Hakan Altan for his valuable suggestions and helps during set up of our system.

I would like to thank also to my colleagues; Mohammad Zabara, Inal Gabunia, Mehmet Volkan Yağın, Mohammad Ali Rahimi, Enis Arık, Ergün Kara, Emine Kaya, Zühra Çınar, Alim Yolalmaz, Muzaffer Gencay Çelik, Hakan Ünay, Gizem Çalışgan, Mustafa Yaşa, Kadyrbek Ismailov, Nurzhan Beksultanova, and all my other colleagues for their kind friendship, encouragement, and support.

I would like to thank to my thesis committee members for honouring my thesis defence and broadening my horizon with their valuable comments and questions.

I would like to acknowledge TUBITAK (111T393) and METU-BAP for the financial support.

Finally, I sincerely thank to my family for their endless support.

## TABLE OF CONTENTS

ABSTRACT .....	v
ÖZ .....	vii
ACKNOWLEDGEMENTS .....	x
TABLE OF CONTENTS .....	xi
LIST OF TABLES .....	xiii
LIST OF FIGURES .....	xiv
LIST OF SYMBOLS AND ABBREVIATIONS .....	xviii
CHAPTERS	
1. INTRODUCTION .....	1
1.1 Terahertz region and radiation.....	1
1.2 Short history .....	3
1.3 THz generation and detection methods .....	3
1.4 Terahertz spectroscopy techniques.....	5
1.5 Applications of THz spectroscopy .....	6
2. EXPERIMENTAL .....	9
2.1 THz-TDS system setup - overview .....	9
2.2 Main parts of the system and their properties .....	11
2.2.1 Laser .....	11
2.2.2 THz wave emitters .....	12
2.2.3 THz wave detectors.....	14
2.2.4 Lock-in amplifier .....	14
2.3 Working principle of the system .....	16
2.4 Data collection and analysis .....	17
2.5 Determination of suitable data analysis software.....	19
2.6 FT-THz instrument used in our studies.....	22
2.7 SNR and DR.....	23
2.8 Sample preparation.....	24
3. SYSTEM SETUP AND OPTIMISATION STUDIES .....	29
3.1 System setups .....	30

3.1.1	Antenna-antenna setup .....	30
3.1.2	Antenna-crystal set-up.....	32
3.2	Sample angle effect .....	39
3.3	Optimisation studies. ....	40
3.3.1	Scan mode and stage speed optimisations.....	40
3.3.2	Lock in parameters optimisation .....	45
3.3.3	Stage hysteresis problem .....	51
3.4	Dry Air Purged Box.....	54
3.5	Optimised System Parameters .....	54
4.	RESULTS AND DISCUSSION .....	57
4.1	THz Spectrum of Water Vapour.....	59
4.2	THz spectra of APIs .....	60
5.	CONCLUSION .....	75
	REFERENCES.....	77

## LIST OF TABLES

<b>Table 1.</b> The equipment of our THz-TDS system .....	9
<b>Table 2.</b> SNR and DR of average of 5 sequential signals .....	24
<b>Table 3.</b> The list of APIs' name formula, and structure .....	25
<b>Table 4</b> Resistance of the antennae .....	31
<b>Table 5.</b> Mean and standard deviation of data given in Figure 32 .....	45
<b>Table 6.</b> Mean and standard deviations of the signals obtained with the different reserve settings.....	47
<b>Table 7.</b> Mean and standard deviations of the time constant dB settings shown in Figure 35 .....	48
<b>Table 8.</b> Mean and standard deviation of noise level obtained with different time constant settings .....	49
<b>Table 9.</b> Mean and standard deviation of the noise level with 100 ms, 300 ms and 1 s time constants .....	51
<b>Table 10.</b> Optimised system parameters.....	55

## LIST OF FIGURES

<b>Figure 1.</b> Terahertz region of the electromagnetic spectrum together with the properties of THz light.....	2
<b>Figure 2.</b> THz beam generation and a) front and b) side view of a PCA .....	4
<b>Figure 3.</b> Optical spectrum of Ti:Sapphire laser operating in (a) CW operation and (b) modelocked.....	11
<b>Figure 4.</b> Images of PCA antenna gap structure .....	13
<b>Figure 5.</b> iPCA antenna structure .....	13
<b>Figure 6.</b> Simplified schematics of electrooptic sampling method for detection of THz radiation. The birefringent crystal (ZnTe in this case) changes visible pulse as shown. This change is caused by the THz pulse. ....	15
<b>Figure 7.</b> Stanford Research System Lock-in Amplifier .....	15
<b>Figure 8.</b> THz-TDS system with antenna generation and EOS detection techniques.....	16
<b>Figure 9.</b> Time domain THz field profile of reference and sample. The sample causes attenuation and intensity decrease on the reference signal.....	19
<b>Figure 10.</b> Faulty behaviour of Origin in analysing frequency intensity of sample and reference in the range of 0.1-0.5 THz. ....	20
<b>Figure 11.</b> In 0.1-0.5 THz the absorption coefficients of pure meloxicam samples are calculated as negative by Origin. ....	21
<b>Figure 12.</b> Interface of the THz Spectrum Viewer.....	21
<b>Figure 13.</b> Comparison of data analysed by a) Origin and b) Terahertz Spectrum Viewer software .....	22
<b>Figure 14.</b> Thermo Nicolet 6700 FT-THz spectrometer .....	22
<b>Figure 15.</b> Average of 5 sequential time domain signals that is used for SNR calculation .....	24
<b>Figure 16.</b> Antenna-antenna system setup.....	32
<b>Figure 17.</b> a) The signal obtained from the antenna-antenna system and b) its frequency components .....	32

<b>Figure 18.</b> Antenna-crystal system setup with one OAPM.....	33
<b>Figure 19.</b> a) The signal obtained with Antenna-crystal system setup with one OAPM and b) its frequency components.....	34
<b>Figure 20.</b> Antenna-crystal system purged with dry air (dash-dotted box).....	35
<b>Figure 21.</b> a) The signal obtained with three OAPM system and b) its frequency components .....	36
<b>Figure 22.</b> Antenna-crystal system with 2 OAPMs. The Teflon lens of the antenna is removed thus 2 OAPMs are needed to focus the light on the detection crystal .....	36
<b>Figure 23.</b> a) THz time domain signal and b) its frequency component obtained by the system .....	37
<b>Figure 24.</b> Final version of the system; 8-F OAPM system.....	37
<b>Figure 25.</b> a) Time and b) frequency domain profiles of THz field obtained by the final 8F configuration of the system. ....	38
<b>Figure 26.</b> Ibuprofen spectra a) collected with our system and b) available in the literature. The literature result belongs to (RS) ibuprofen which was analysed at both 78 and 293 K.....	39
<b>Figure 27.</b> a) Sample rotation experiment with angles of ca. 0, 20 and 45 degrees b) FFT results of the rotation of sample experiment .....	40
<b>Figure 28.</b> a) Signal profiles and b) bandwidth of different stage speeds (40 pps solid line, 50pps dashed line, 60pps dotted line and 70 pps dash-dotted line) .....	41
<b>Figure 29.</b> Absorption spectra of Losartan potassium collected at different stage speeds by THz-TDS and FT-THz systems. The spectra are shifted for clarity. ....	42
<b>Figure 30.</b> a) Signal profiles and b) bandwidth of different stage step sizes (1 $\mu$ m solid line, 3 $\mu$ m dotted line and 6 $\mu$ m dashed line).....	43
<b>Figure 31.</b> Comparison of step and continuous modes with different stage speeds .....	44
<b>Figure 32.</b> Time profile collected with AC coupled, DC coupled and Float settings of lock-in amplifier.....	45
<b>Figure 33.</b> a) Time domain profile with several sensitivity settings of lock-in b) FFT of the signals given in a. ....	46
<b>Figure 34.</b> Time profiles at 3 different reserve settings of lock-in.....	47

<b>Figure 35.</b> Time constant dB settings of lock-in .....	48
<b>Figure 36.</b> Signal of the noise floor obtained with different time constants .....	50
<b>Figure 37.</b> Effect of averaging on results with 100, 300 ms and 1 s time constants .....	50
<b>Figure 38.</b> The effect of time constant on the achievable bandwidth of Losartan potassium. The speed of the stage was equal or each of 100 ms and 300 ms time constants (80pps).....	51
<b>Figure 39.</b> a) Multiple scans of normal scanning mode without any outside intervention. b) Bringing the stage manually to a position that is on the left hand side of the initial point. The stage normally comes to the initial point from the right hand side. c) Manual positioning of the stage to the initial position of the scan .....	52
<b>Figure 40.</b> a) Normal scan in step scanning mode. b) Manual initial positioning of stage in step mode.....	53
<b>Figure 41.</b> Bandwidth change before and after having dry air in the system. The strong water vapour bands present at 39 and 57 $\text{cm}^{-1}$ and the relatively weak band at 18 $\text{cm}^{-1}$ totally disappears.....	54
<b>Figure 42.</b> THz transparencies of a) polymethylpentene (TPX) and b) high density polyethylene (HDPE) .....	58
<b>Figure 43.</b> Comparison of different type of PE in terms of transmission properties.....	58
<b>Figure 44.</b> Absorption spectrum of water vapour.....	59
<b>Figure 45.</b> a) Frequency dependent absorption coefficient and refractive index of pure Meloxicam. b) Simulated spectra of enol (red) and cationic(blue) forms overlaying under the baseline corrected meloxicam spectrum. ....	60
<b>Figure 46.</b> a) THz spectra of pure, 5 %, 7 %, and 10 % (w/w) Meloxicam in PE. The spectra of mixture samples were multiplied by 3 for clarity b) FT- THz spectrum of 5 % meloxicam over the range of 1.5 to 20 THz. ....	63
<b>Figure 47.</b> THz transmission study of drug host materials (box, plastic blister) a) time domain b) frequency domain data. ....	63
<b>Figure 48.</b> Spectra of 10 % and 5 % (w/w) Ibuprofen sample obtained by a) THz-TDS with samples (10 % and 5 % w/w) and b) FT-THz (5 % w/w) techniques.....	65
<b>Figure 49.</b> Spectra of 5 % w/w Benzocaine sample obtained by a) THz-TDS) and b) by FT-THz. ....	66

<b>Figure 50.</b> Spectra of Fluoxetine HCl sample obtained by a) THz-TDS (10 % w/w) and b) FT-THz (5 % w/w) .....	67
<b>Figure 51.</b> Spectra of 5 % (w/w) Irbesartan sample obtained by a) THz-TDS) and b) by FT-THz .....	68
<b>Figure 52.</b> Spectra of 2 % and 5 % (w/w) Losartan Potassium sample obtained by a) THz-TDS (2 % and 5 % w/w) b) FT-THz (5 % w/w).....	69
<b>Figure 53.</b> Spectra of Paracetamol sample obtained by a) THz-TDS (2 and 5 % w/w) b) FT-THz (5 % w/w).....	70
<b>Figure 54.</b> Spectra of 2 and 5 % (w/w) Ranitidine HCl sample obtained by a) THz-TDS (2 and 5 % w/w) and b) FT-THz (2 % w/w).....	71
<b>Figure 55.</b> Spectra of 5 % (w/w) Cinnarizine sample obtained by a) THz-TDS) and b) FT-THz. ....	72
<b>Figure 56.</b> Spectra of 5% (w/w) Desloratadine sample obtained by a) THz-TDS) and b) FT-THz .....	73
<b>Figure 57.</b> Spectra of 5 % (w/w) Telmisartan sample obtained by a) THz-TDS and b) FT-THz .....	74

## LIST OF SYMBOLS AND ABBREVIATIONS

THz	: Terahertz
GHz	: Gigahertz
THz-TDS	: Terahertz Time Domain Spectroscopy
FT-THz	: Fourier Transform Terahertz Spectroscopy
PCA	: Photoconductive Antenna
iPCA	: Interdigital Photoconductive Antenna
SNR	: Signal-to-noise ratio
DR	: Dynamic range
Ti:Sapphire	: Titanium Sapphire
GaAs	: Gallium Arsenide
ZnTe	: Zinc Telluride
FFT	: Fast Fourier Transform
fs	: Femtosecond
pps	: Points per picosecond
API	: Active Pharmaceutical Ingredient
OAPM	: Off-axis parabolic mirror
TES	: Terahertz Emission Spectroscopy
TRTS	: Time resolved Terahertz Spectroscopy
eV	: Electronvolt
mW	: Milliwatt
ms	: Millisecond
dB	: Decibel
AC	: Alternating current
DC	: Direct current
CW	: Continuous waveform

GaAs	: Gallium Arsenide
InAs	: Indium Arsenide
InP	: Indium Phospide
LiNbO <sub>3</sub>	: Lithium Niobate
HDPE	: High Density Polyethylene
TPX	: Polymethylpentene



## CHAPTER 1

### INTRODUCTION

#### 1.1 Terahertz region and radiation

Terahertz (THz) region of the electromagnetic spectrum lies in between the microwave and the far infrared regions that generally corresponds to a frequency range from 100 GHz to 10 THz. The name of the region originates from the prefix of the frequency unit, hertz. The word ‘tera’ is derived from a Greek word meaning ‘monster’; however, it is the prefix having the meaning of ‘multiply by  $10^{12}$ ’ in metric system. As presented in **Figure 1**, 1 THz has the equivalences of  $33.33 \text{ cm}^{-1}$  wavenumber,  $300 \text{ }\mu\text{m}$  wavelength, and 4.1 meV photon energy. THz photon energy is in the range of rotational transitions of molecules, vibrational transitions including both intra and intermolecular, hydrogen bonded molecular motions, molecular torsions. In this region there are wide range of phenomena that could be investigated by engineers and scientists; however, it has not been very convenient to reach this region of the electromagnetic spectrum due to technical difficulties. That is why this region is generally referred as ‘terahertz gap’ until recently. Photon energy of 4.1 meV is much less than that of visible and near IR photons which has photon energy on the order of eV thus it is so improbable that the sample would decompose due to THz radiation. This makes the application of THz spectroscopy quite safe. Even semiconductor materials do have band gap energies on the order of eV, corresponding to an energy of one thousand times larger than terahertz energy. [1]

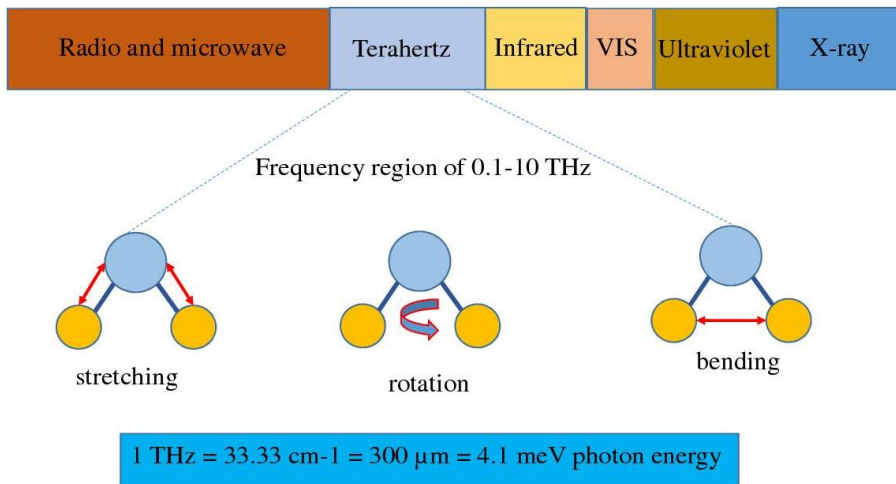


**Figure 1.** Terahertz region of the electromagnetic spectrum together with the properties of THz light.

For the sake of producing THz radiation, scaling the optical or electronic devices has not been an efficient way since there are some restrictions. Firstly, modification of the electronic devices to work in terahertz frequencies is quite limited especially for high frequencies (>1THz) due to the limited frequency response of the devices.[2] This response depends on the time duration at which electrons pass through the device, relying on the physical size and carrier mobility. Therefore, the material used is very important because it determines the high frequency response.[2] On the other hand, it is not an efficient way to employ optical sources to operate at terahertz frequencies because they also have limited frequency ranges.[2] There are blackbody sources working in THz region incoherently but it is very difficult to detect this radiation because there is always incoherent thermal background signal which cause interference with the actual one.

Instead, in time, the researchers have developed other techniques like employing free electron lasers, synchrotrons, narrowband quantum cascade lasers, broadband generation from ultrafast pulsed lasers to generate THz light in a coherent manner with good SNR ratios.

## 1.2 Short history

There have been several attempts to produce THz radiation in the history but radical change occurred between 1988 and 1989. The researchers Daniel Grischkowsky, David Auston, and Martin Nuss managed to emit and detect THz pulses through free space from a generator.[3], [4] Since then the number of researchers working on this topic have increased and THz spectroscopy or technology become widespread all over the world. Some of the research areas of terahertz technology involves the areas of solid state physics, biology, pharmaceuticals, and security screening.[5]–[13] With the recent advancements in technology, it is possible now to conduct experiments in time domain in which there is no need for special detectors.[2] Furthermore, time resolved studies also became possible where dynamic properties of substances are investigated.[7], [8], [14]

## 1.3 THz generation and detection methods

Two of most commonly employed generation techniques are going to be mentioned in this thesis. The first one, photoconductive switching, uses oscillator lasers while the second one, optical rectification generally needs amplifier based systems.

A photoconductive antenna is basically composed of two parts; a photoconductor and metal plates. Among typical photoconductors there are high resistivity GaAs, InP and radiation damaged silicon wafers. Antenna structure is constructed by having two metal electrodes, supplying the bias voltage to the gap between them as shown in **Figure 2a**. In this method, an ultrafast laser is used having pulses with energies in the vicinity of the bandgap energy of the photoconductor. Those pulses cause excitation of electrons to the conduction band leaving hole behind. Then, applied bias voltage causes these free carriers to accelerate to form a transient photocurrent. This acceleration of carriers results in radiation in THz frequencies.[15]

There are some factors that limits the intensity and bandwidth of the generated THz pulse. Firstly, the employed material should have rapid photocurrent rise and decay times. InAs and InP seem to respond to this need well with their small effective

electron masses. Also, the breakdown field of the material is important because maximum bias voltage is determined by this property of the material.[15]

The THz light produced by using this technique propagates through both parallel and antiparallel to the incoming laser radiation. Mostly the parallel beam that is propagating in the direction of the laser beam used in studies; however, the backward radiation could also be used. The THz radiation produced in forward and backward directions are presented in **Figure 2b**. The backward radiation is superior to the forward radiation such that it results in minimal dispersion of THz pulses, thus having extensive bandwidth[16].

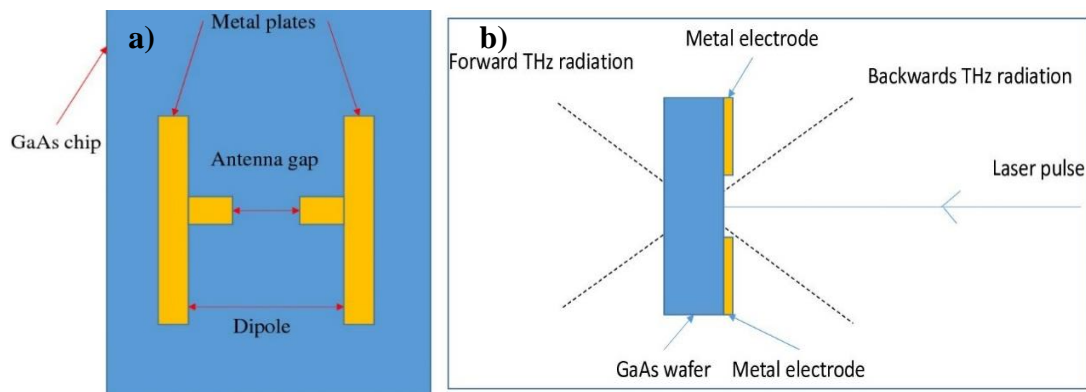


**Figure 2.** THz beam generation and a) front and b) side view of a PCA

Optical rectification is another commonly employed THz radiation generation technique. In this technique a non-linear crystal is exploited and second order non-linear optical effect is observed. There is no bias voltage applied in this method but the high intensity laser pulse coming to the crystal results in generation of the THz radiation by conversion of frequencies.[15] This conversion of frequencies is limited by the non-linear coefficient of the non-linear crystal and phase matching conditions.

If we briefly compare the two generation techniques, photoconduction provides higher output power while optical rectification could produce broader bandwidth up to 50 THz.[17]

Among the THz detection systems, photoconductive antennae and electro-optic sampling methods are the two most commonly used techniques for coherent detection. Firstly, photoconduction shares the same principles with THz generation. Oscillator laser populates the conduction band with its broadband pulses. However, different from the THz generation by PCA, the acceleration of the carriers is achieved by the THz field itself and there is no bias applied to the antenna. This acceleration of the carriers results in transient photocurrent. By means of a delay line, relative arrival time of the THz and visible pulses is changed and the electric field of the THz pulse is mapped out as a function time.[18]

Furthermore, the second technique is called electrooptic sampling in which an electro optic crystal like ZnTe or LiNbO<sub>3</sub> is employed. The generated THz beam is guided generally by off-axis parabolic mirrors (OAPMs) and finally is focused onto this crystal. At the same time, the probe beam also passes through this crystal. The THz beam causes birefringence on the crystal and this in turn causes change in polarisation of the probe beam. The alteration amount is proportional to the THz field strength. This polarisation alteration is detected by the balance photodiode detector with the help of quarter waveplate, Wollaston prism, and lock-in amplifier. By changing the gating time of the visible and THz pulses, the THz pulse profile is obtained in time domain.

#### **1.4 Terahertz spectroscopy techniques**

Three of the most commonly used THz techniques will be explained here briefly. That are Terahertz Time Domain Spectroscopy THz TDS, Terahertz Emission Spectroscopy (TES), and Time Resolved Terahertz Spectroscopy (TRTS). THz-TDS is the most common one among them. Except for TRTS, the other techniques provides static properties of samples[19], such as absorption coefficient, refractive index, that are needed for applications in molecular spectroscopy, biology, and quality control. On the other hand, TRTS measures the dynamic properties of the materials.[7], [14], [20]

In THz-TDS technique measurements are done in the following fashion: subpicosecond THz pulses are produced with the help of photoconductive antenna or

a non-linear crystal. Then, for transmission mode, these pulses are allowed to pass firstly through a reference with known properties. Afterwards, the sample is placed into the light propagation path and the pulses experience alterations in terms of intensity and phase due to the presence of a different medium. After obtaining the signals in time domain, FFT is applied to have frequency domain spectra of both reference and sample. Finally, this converted frequency domain signal of reference and the sample are used to extract optical properties of the sample under investigation. [19]

TRTS is a bit more complicated compared to THz-TDS. In TRTS, the laser beam is split into three, one is for THz generation, one is for pumping the sample, the last one is for detection of THz signal. A sample is photoexcited by using an ultrafast pump pulse, having a wavelength generally ranging from UV to mid-IR. Afterwards the change in THz transmission is measured as a function of time. The obtained signal gives the information of both photoconductivity and excitation lifetime about the sample. Photoconductive studies are among the most important applications of TRTS. This technique is an important tool for non-contact analysis of semiconductors with high resolution. [7]The technique may also be used for following dynamic processes such as reactions, conformational transformations, morphological changes, etc. However, such applications are currently very limited due to very low SNRs.[21]

Terahertz Emission Spectroscopy is another technique used for analysis of bulk semiconductors, semiconductor heterostructures like quantum wells and superlattices, superconductors, organic molecules.[22]–[24] It shares similar properties with a typical THz-TDS. In TES, the sample is exposed to pulsed laser radiation to be photoexcited and as a result the sample emits THz radiation. Then the transient electric field radiated from the sample is measured for analysis.[2]

### **1.5 Applications of THz spectroscopy**

THz radiation draws great attention with its unique properties such as being able to penetrate non-invasively into non-metals like paper, plastic, many synthetics and textiles. Since the fingerprints of materials also lie in THz region both identification and characterisation of materials are possible even if the sample is covered with THz transmissive materials like paper, plastic, etc. Application areas of THz waves have

been as divergent as molecular spectroscopy[25], solid state physics[9], [11] , biology[6], [12], pharmaceuticals[26]–[28], imaging[29] and even art conservation[30]. Especially in pharmaceuticals, it is gaining significant attention because of its potential in quantifying[27], [31], identifying and discerning[32] drugs even if they possess more than one polymorphic form.

In pharmaceutical industry one of the main effort is set for obtaining drugs with optimum bioavailability, stability and solubility besides its efficacy. Any change in molecular structure (even transitions within the polymorphic forms) prior to, during or after manufacturing of the drug may result in an unwanted change in solubility, bioavailability, dissolution rate in addition to possibly becoming a danger to human health[33]. Therefore, characterisation techniques play a significant role in every part of the manufacturing processes. Common techniques used in drug analysis are X-ray diffractometry, differential scanning calorimetry, IR and Raman spectroscopies and solid state NMR.[34]–[36] THz spectroscopy is an emerging and very promising new technique in this field. With its aforementioned advantages it is expected to be a complementary technique to the current ones. Its ability to measure the analyte right in the packaging, moreover, does bring an additional advantage to in situ characterisation of drug especially when it is at a shelf.

The most common pharmaceutical dosage of a drug is tablet. A tablet mainly contains the drug and inert fillers and binders called excipients. Tablets are being analysed before, during, and after manufacturing for content, quantity, and homogeneity. Prior to production form of active pharmaceutical ingredient (API) and bulk pharmaceutical chemicals (excipients) are checked and conformed. During the mass production, tablets are also tested for any change in the form of API when necessary. Tablets may also be checked for having right amount of coating material for controlled release of the drug or to protect for degradation due to harsh acidic conditions of the stomach, etc. Furthermore, tablets are also analysed for shelf life prior to marketing under simulated market conditions since an API may have limited stability and may change its form during storage. Additionally, if possible, it would be necessary to characterize finished pharmaceuticals right at the shelf on the market for further degradation due to the market storage conditions. There has been no such technique that can be used in

all of these steps; however, THz spectroscopy appears to be really good candidate to monitor tablets or drugs before, during, and after manufacturing processes for its morphology, homogeneity, and the tablet coating quality. Recent studies have shown the capability of THz spectroscopy to identify polymorphs and characterise API [5], [13], [26]–[28], [31], [32], [37]–[47] and to measure tablet coating thickness[48]. With its penetrating and non-destructive nature, THz spectroscopy allows to analyse a drug even in its packaging without a need for a destructive procedure. This is an important advantage for determination of shelf-life of a drug under various storage conditions or directly at market shelf when the technology is available.

## CHAPTER 2

### EXPERIMENTAL

#### 2.1 THz-TDS system setup - overview

THz-TDS is becoming a widely applied tool for identification, characterisation, and detection of materials or molecules. The main aim of the studies in this thesis was building a THz-TDS spectroscopy system. For this purpose, five systems have been setup with varying configurations. The final version of the system is an 8F Terahertz Time Domain Spectrometer, which mainly utilises an ultrafast Ti:Sapphire oscillator laser as a light source, a photoconductive switch as THz emitter, and a birefringent crystal, ZnTe, of <110> orientation and 500  $\mu\text{m}$  thickness as detector. Our system is composed of the equipments given in **Table 1**.

**Table 1.** The equipment of our THz-TDS system

Item	Manufacturer	Model	Properties
Ti.Sapphire Mode-locked laser	Coherent	Mantis-5	80 fs pulse duration, 80 nm pulse width, 80 MHz repetition rate, 800 nm central wavelength, 550 mW output power
iPCA antenna	BATOP	iPCA-21-05-1000-800-h	0.5W-3W optimum optical working power, $\pm 15$ V maximum applicable bias voltage
Wollaston prism	Thorlabs	WP10	

**Table 1** continued

PCA antenna	BATOP	PCA-40-05-10-800-h-1	15 mW maximum working optical power, $\pm 10$ V suggested bias voltage
ZnTe crystal	MTI corp		<110> orientation and 500 $\mu\text{m}$ thickness
Quarter waveplate	Thorlabs	WPQ10M-808	
OAPMs			90 deg, f= 15cm, 6cm, 5cm and 2.5 cm
Dielectric mirrors	Thorlabs	BB1-E03	
Beam splitter	Thorlabs	BSF10-B	90:10
Lenses	Thorlabs	LA1908-B and LA1172-B	f= 50 and 40 cm
TPX plate			beam splitter
Large Area Balanced photodiode	Thorlabs	PDB-210-A	
Function generator	HM8030-6	HM8030-6	$\pm 20$ V
Motorised microstage and its controller	Standa	8MT167-100 and 8SMC1-USBHBF-B2-2MC)	
Voltage amplifier	BATOP		48 V
Oscilloscope	Tectronix	DPO2014	
Lock-in amplifier	Stanford Research Systems	45347A	
Multifunction Data Acquisition	National Instruments	NI USB 6251 and USB X SERIES 6361	

## 2.2 Main parts of the system and their properties

### 2.2.1 Laser

An ultrafast Ti:sapphire oscillator laser producing ultrashort pulses was used as optical light source. This solid state laser has gain medium of Titanium doped sapphire ( $\text{Al}_2\text{O}_3$ ) with  $\text{Ti}^{3+}$ . This crystal is pumped by a green diode laser having wavelength of 532 nm and 5.5 W pump power. As a result, a CW radiation having 800 nm central wavelength and ca. 400 mW output power is obtained. (**Figure 3a**) Also, a broadband output is obtained having 80 nm FWHM and ca. 600 mW and 80 MHz repetition rate and 80 fs pulse duration after modelocking the laser as presented in **Figure 3b**.

These type of lasers are so sensitive that the ambient conditions (dust in the air, humidity temperature, etc.) should be stable in order to operate the laser. Thus, there is a sophisticated air conditioning system and a chiller that are used to provide proper working conditions for the laser. The air conditioning system is able to sustain the temperature nearly stable at desired temperature by providing constant circulation of the air inside the lab. Apart from cooling, this system also filters the circulating air in order to eliminate the dust particles present in the air, which affect the laser negatively by reducing the reflectance of the mirrors inside the laser.

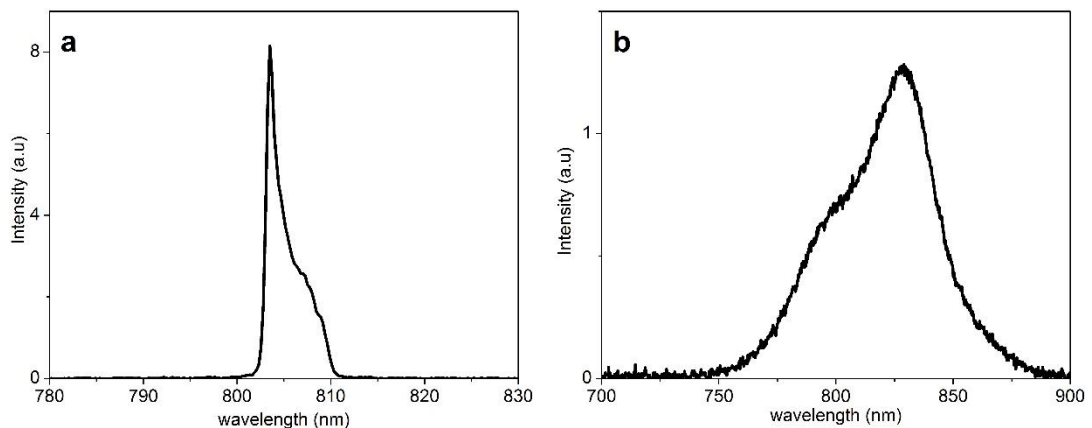


**Figure 3.** Optical spectrum of Ti:Sapphire laser operating in (a) CW operation and (b) modelocked.

There is also a chiller used which cools the laser with the help of a cooling liquid (distilled water). The crystal should be kept cooled otherwise it would not work properly due to the overheating caused by the pump laser. This chiller works at 21 °C and the coolant liquid should be changed every month.

It is not always possible to perfectly sustain the conditions, therefore, the laser requires some other procedures for optimum working like alignment of the light in the laser and cleaning the optics inside the laser. As mentioned earlier, the temperature is crucial for laser stability. Even 1.0 °C change in temperature does result in significant drop in laser output power. The mirrors change their positions in micro scales as a result of temperature change which in turn changes the sensitive alignment of the cavity, which is made up of 14 mirrors.

### **2.2.2 THz wave emitters**

We have used two type of photoconductive antennae to generate THz light, PCA-40-05-10-800-x and iPCA-21-05-1000-800-h. In principle, both antennae could be used for both generation and detection of THz radiation.

The PCA antenna has Au electrodes deposited onto GaAs semiconductor chip (**Figure 4**). Two electrodes of 'L' shape brought together to form a gap of 5  $\mu\text{m}$  in width. The red circle indicates the 5  $\mu\text{m}$  antenna gap. The working principle of the antenna is as follows; the laser beam having photon energy larger than the antenna energy gap  $E_g$ , is focused onto this antenna gap by a suitable objective. This focusing of the beam causes the carriers to be excited to conduction band of the GaAs. The excited carriers are then accelerated by an applied bias voltage (ca. 10 V for this antenna), and this acceleration results in THz radiation.[18]

This antenna requires 10 mW of optical power and 10 V of bias voltage for optimum working. Our antenna already had a lens attached to focus the light onto the antenna gap thus we did not require an objective to have the light focused. However, the performance of the antenna was much less than expected.

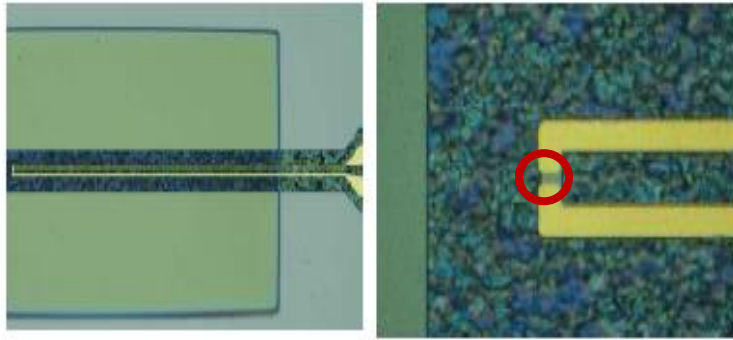


**Figure 4.** Images of PCA antenna gap structure [49]

On the other hand, iPCA antenna possesses different structure compared to PCA antenna. It has more than one antenna gap formed by finger electrodes lie on the antenna chip, as can be seen in **Figure 5**. The antenna has array of lenses on itself to focus the light onto the antenna gaps. The working principle can be said to be the same with PCA antenna; however, the parameters required is different such that 0.5-3 W of optical power and 15 V of bias voltage is required. Also the incoming laser beam to the antenna should have a diameter around 1 mm and should be collimated. In this study, the antenna was operated at 14 V voltage and ~450 mW optical power. Also a lens of 50 cm focus is being used to have almost collimated light reaching to the antenna.

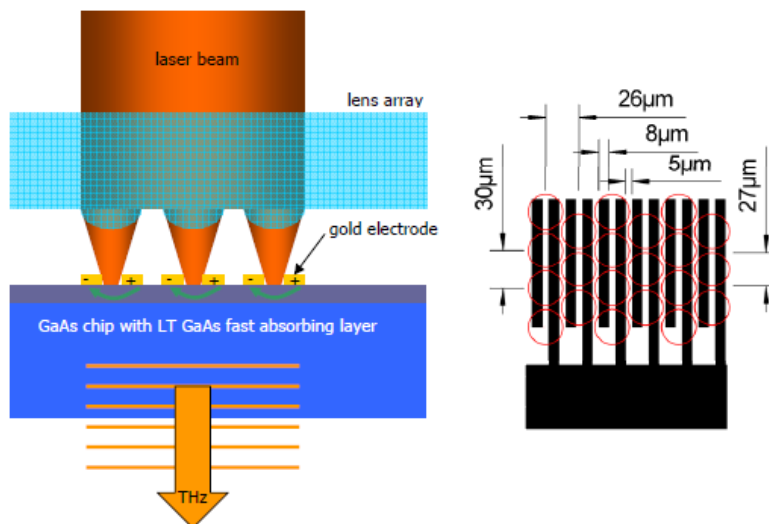


**Figure 5.** iPCA antenna structure [50]

### 2.2.3 THz wave detectors

The similar antennae, iPCA or PCA, can also be used to detect THz radiation and we have employed both of them for detection purposes. They work in similar fashion as they generate THz radiation with slight differences in use of optical light. Here, optical pulse act as bias and accelerates the carriers. As mentioned earlier, the acceleration causes a transient current which is recorded by the help of lock-in amplifier as THz signal[18].

There is also electrooptic sampling technique for THz detection. For this technique we used a birefringent 500  $\mu\text{m}$  thick  $\langle 110 \rangle$  ZnTe crystal to detect THz radiation. In this technique, the THz beam is guided by off-axis parabolic mirrors (OAPMs) after being generated, and finally is focused onto this crystal. At the same time the probe beam also passes through this crystal. The THz beam causes birefringence on the crystal and this in turn causes polarisation change of probe beam. This polarisation alteration is detected by the balance photodiode detector with the help of quarter waveplate and Wollaston prism. By changing the gating time of the visible and THz pulses, the THz pulse profile is obtained in time domain.[51] The detection process is illustrated in **Figure 6**.

### 2.2.4 Lock-in amplifier

**Figure 7** belongs to a typical lock-in amplifier. A lock-in amplifier is used to detect signal regardless of low intensity of signal, as low as nanovolts. It can extract very low signal from its noisy background even though the noise level is thousand times or even larger in intensity[52]. Lock in amplifiers need a specific reference frequency and phase to provide the sought signal. This is achieved by a phase sensitive detector.

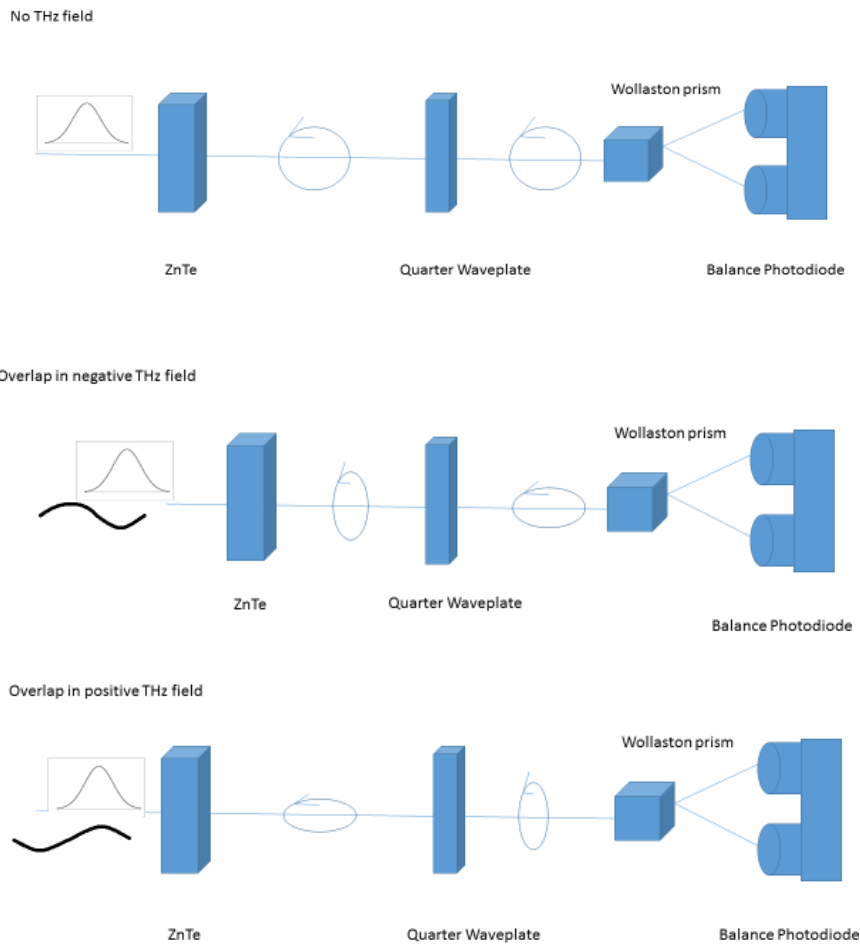


**Figure 6.** Simplified schematics of electrooptic sampling method for detection of THz radiation. The birefringent crystal (ZnTe in this case) changes visible pulse as shown. This change is caused by the THz pulse.



**Figure 7.** Stanford Research System Lock-in Amplifier[53]

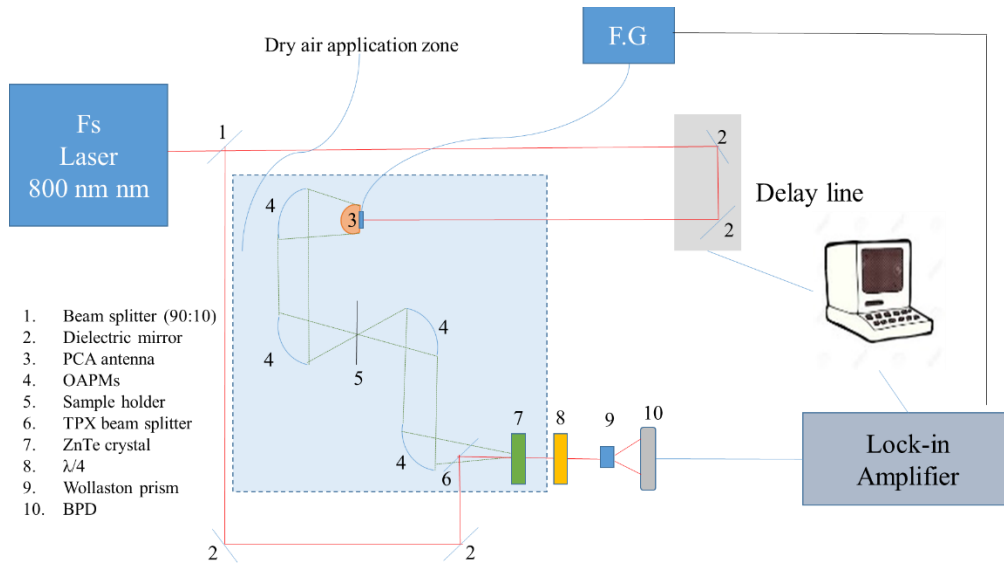


**Figure 8.** THz-TDS system with antenna generation and EOS detection techniques

### 2.3 Working principle of the system

The **Figure 8** belongs to the setup present in our lab. A femtosecond laser is used for both THz generation and detection purposes. The generated THz beam is guided with the help of 8F off-axis parabolic mirrors set-up to focus the beam onto the sample. After passing through the sample, the THz beam is focused onto a non-linear ZnTe crystal for detection. The probe beam passes through the detection crystal to sense THz radiation by the technique called electro-optic sampling.[51] By changing the gating time of the THz and visible pulses to the ZnTe crystal, THz beam profile is obtained with the help of quarter waveplate, Wollaston prism, balance photodiode, lock in amplifier and a computer.

The aim of use of quarter waveplate and Wollaston prism couple is for monitoring any change in beam polarisation, thus detection of THz light. The quarter waveplate is able to change the polarisation of the light and the Wollaston prism splits the light according to polarisation (s or p). In the system, the position of quarter waveplate is prior to Wollaston prism according to propagation of light. Initially, when there is no THz light, the polarisation of the visible light reaching to the balanced photodiode is changed such that it has equal intensities at s and p polarisations. When THz beam

arrives to the crystal, it causes birefringence on the crystal thus the crystal changes the polarisation of visible light. This change disturbs the initial balance of the photodiodes. The amount of change in the polarisation is proportional to the field strength thus monitoring this change in time domain records THz radiation in time by scanning the delay stage.

## **2.4 Data collection and analysis**

As mentioned above, overlap of THz pulse and probe pulse in time domain on ZnTe crystal causes polarisation change in probe pulse because THz beam results in birefringence on the ZnTe crystal. This polarisation change is detected by a balanced photodiode, quarter waveplate, Wollaston prism and lock-in amplifier. Function generator and balanced photodiode are connected to the lock-in amplifier. Microstep translation stage is controlled by a Labview code. This software enables us to operate the stage in both continuous and step scan modes. Since we have found out continuous scan to be more advantageous (the details are given later) in terms of providing good signal and practical averaging of sample signal, features of this mode will be mentioned. In continuous scan mode, the software provides the time domain profile of the electric field scanned with certain window size and velocity of the microstep stage. The number of points is constrained by the time constant setting of the lock-in amplifier and the total number of data points in the scan window. The current settings are 150 point per picosecond (pps) distance travelled by the translational stage. The step size of the stage and scan length determines the bandwidth and resolution of the signal to which FFT is applied according to the equations given below. This setting with 100 ms time constant on the lock-in amplifier gave the best SNR with a reasonable scan time of 3 minutes.

The lock-in amplifier gathers information from function generator and the balance photodiode and transfers the information to Labview through a data acquisition card (DAQ) while the function generator applies bias voltage to the antenna, balance photodiode informs lock-in about the transient voltage of THz signal and Labview gathers all this information and collects the data.

Our scan settings are; 13 ps windowing with 1950 data points. The lock-in amplifier was set on 100  $\mu\text{V}$  voltage, 100 ms and 24 dB time constant, 500  $\mu\text{V}$  sensitivity, normal reserve setting, and 2x line filters.

The time domain signals of both reference and sample is obtained by changing the time delay between THz and probe pulses with help of a delay line controlled by Labview software. THz pulse profile for both a reference and a sample is shown in **Figure 9**. The presence of the sample causes delay, attenuation and dispersion on the mapped THz pulse.

The following equations are used to extract optical properties of materials, absorption coefficient, refractive index and complex dielectric constants, which are stated as;

$$n = 1 + \frac{c(\phi - \phi_0)}{\omega d} \quad 1$$

$$\alpha = -\frac{1}{d} \ln\left(\frac{P}{P_0}\right) \quad 2$$

$$\hat{n} = n + ik \quad 3$$

$$k = \frac{\lambda \alpha}{4\pi} = \frac{c\alpha}{2\omega} \quad 4$$

$$\hat{\epsilon} = \hat{n}^2 \quad 5$$

$$\epsilon' = n^2 + k^2 \quad 6$$

$$\epsilon'' = 2nk \quad 7$$

where  $n$  is refractive index,  $\alpha$  is absorption coefficient,  $\hat{n}$  is complex valued refractive index,  $\lambda$  is wavelength,  $P$  is power,  $\phi$  is phase,  $c$  is speed of light in vacuum,  $\omega$  is angular frequency,  $d$  is thickness of the sample,  $k$  is extinction coefficient,  $\hat{\epsilon}$  complex valued permittivity,  $\epsilon'$  is real component of permittivity, and  $\epsilon''$  is imaginary component of permittivity.

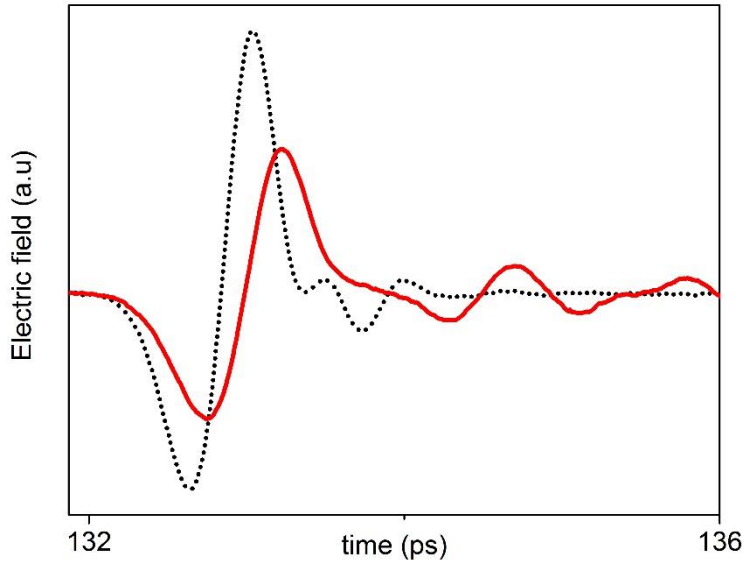


**Figure 9.** Time domain THz field profile of reference and sample. The sample causes attenuation and intensity decrease on the reference signal

## 2.5 Determination of suitable data analysis software

Since the data collected is in time domain, time domain data should be converted to frequency domain in order to have optical properties of the samples. For this conversion, a suitable data analysis software is needed. There are several softwares for this purpose and Matlab, Mathematica, Excel, Origin are among the most commonly employed software for data analysis. However, after some usage, I have realised that Origin results are not the best for absorption coefficient and refractive index calculations. We realised that after we applied FFT to a data collected, there were abnormalities in absorbance of the sample in the frequency range between 0.1-0.5 THz resulting in negative absorption in the spectrum. (**Figure 10** and **Figure 11**) The problem was that the intensity of the reference was lower than that of sample in 0.1-0.5 THz range, which is improbable. Initially we suspected that 8.0 version of the software was unable to apply FFT properly and decided to try other demo versions like; 8.5, 9.0 and 2015. Unfortunately, none of the Origin versions was able to solve the problem thus we searched for another software. There was another option which is readily designed to analyse THz-TDS data, named as THz spectrum viewer developed

by Hiromichi Hoshina[54]. This software is very useful such that it can apply FFT, calculate refractive indices and absorbance practically and in a short time. Also, zero padding and choosing of window type (boxcar, blackman, etc.) are possible using the software. The interface of the software is presented in **Figure 12**.

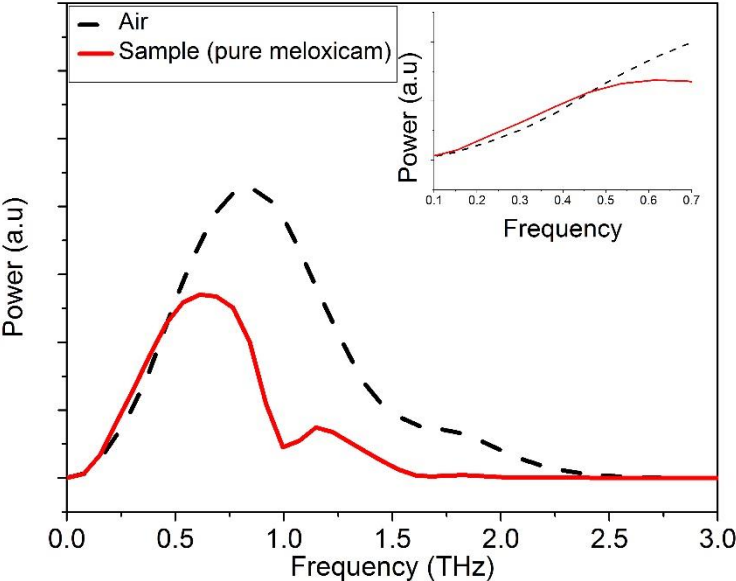


**Figure 10.** Faulty behaviour of Origin in analysing frequency intensity of sample and reference in the range of 0.1-0.5 THz.

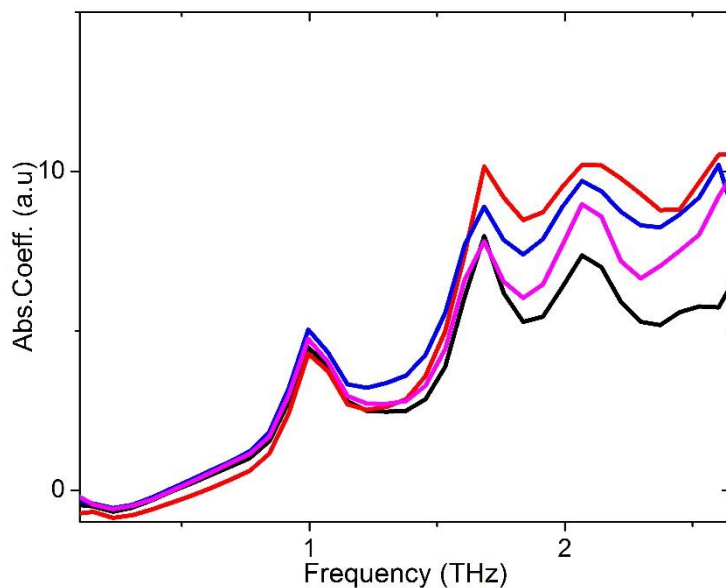


**Figure 11.** In 0.1-0.5 THz the absorption coefficients of pure meloxicam samples are calculated as negative by Origin.

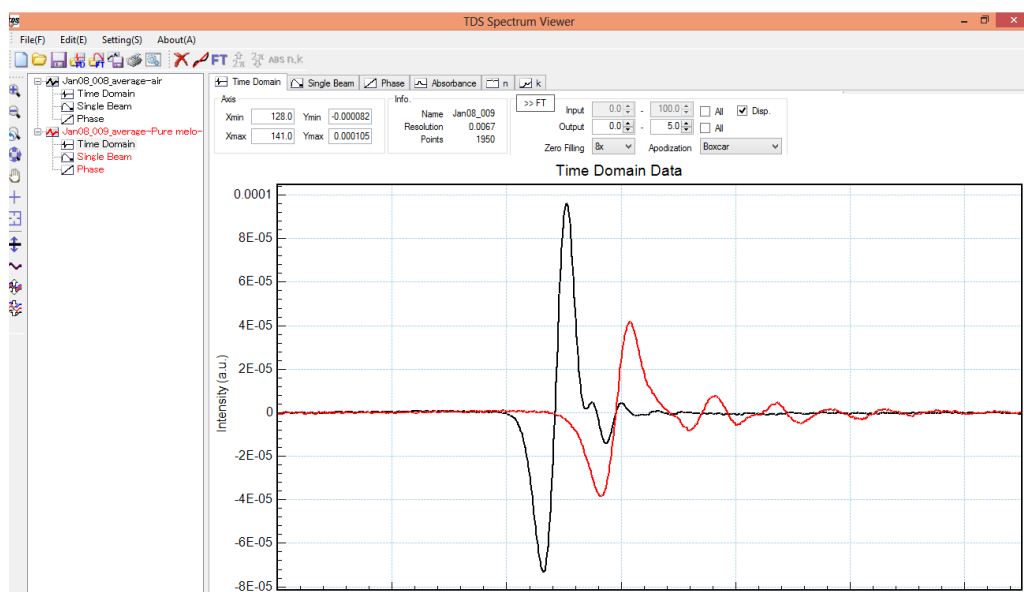


**Figure 12.** Interface of the THz Spectrum Viewer.

The **Figure 13** presents the analysis of the same data (Jan 8, 2016) obtained with two different software; Origin (on the left) and the THz Spectrum Viewer (on the right).

The Origin results in negative absorption of the sample in 0.1-0.5 THz region, which is nearly impossible.

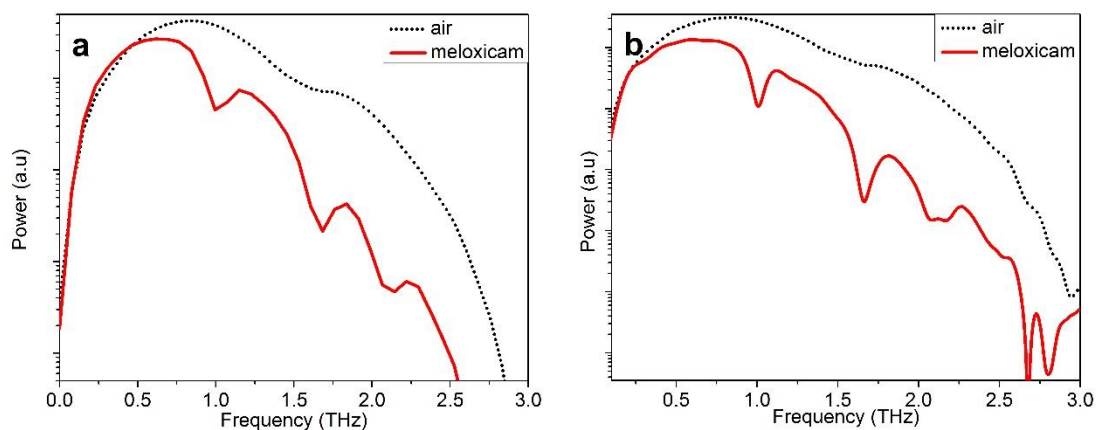


**Figure 13.** Comparison of data analysed by a) Origin and b) Terahertz Spectrum Viewer software

## 2.6 FT-THz instrument used in our studies

All FT-THz measurements were carried out by Thermo Nicolet 6700 FT-THz spectrometer (**Figure 14**) with an effective working range of  $50\text{-}700\text{ cm}^{-1}$ . The spectra are collected in dry air purged environment. It has ETC light source, Si coated mylar beam splitter and DTGS PE detector.



**Figure 14.** Thermo Nicolet 6700 FT-THz spectrometer

## 2.7 SNR and DR

SNR corresponds to the minimum detectable signal whereas DR indicates the maximum quantifiable signal change. There are distinct methods to relate those terms to TDS thus there is no agreed standard over their definition. A good study related to this issue could be found in reference[55]. The SNR and DR of a system in which amplitude is measured could be found as follows;

$$\text{SNR} = \frac{\text{mean magnitude of amplitude}}{\text{standard deviation of amplitude}} \quad 4$$

$$\text{DR} = \frac{\text{maximum magnitude of amplitude}}{\text{rms of noise floor}} \quad 5$$

SNR and DR could be obtained by using either time domain signal or the spectrum obtained by applying FFT. There is no analytical method for relating SNR and DR from time and frequency domain data. Thus the results obtained are specific to time or frequency data. Recommended pathway to obtain SNR and DR is as follows[55];

- 1- Measure the time-domain trace and note the value of the peak maximum.
- 2- The mean signal in the absence of THz should be constant (zero for electro-optic detection, nonzero for a photoconductive antenna). Calculate its standard deviation.
- 3- Measure the peak amplitude over time
- 4- Calculate the standard deviation of the peak amplitude
- 5- Calculate DR
- 6- Calculate SNR

The **Figure 15** presents an average time domain data as an example. The standard deviation of the amplitude is equal to the standard deviation of the noise floor; therefore, the SNR can be assumed to be equal to DR.

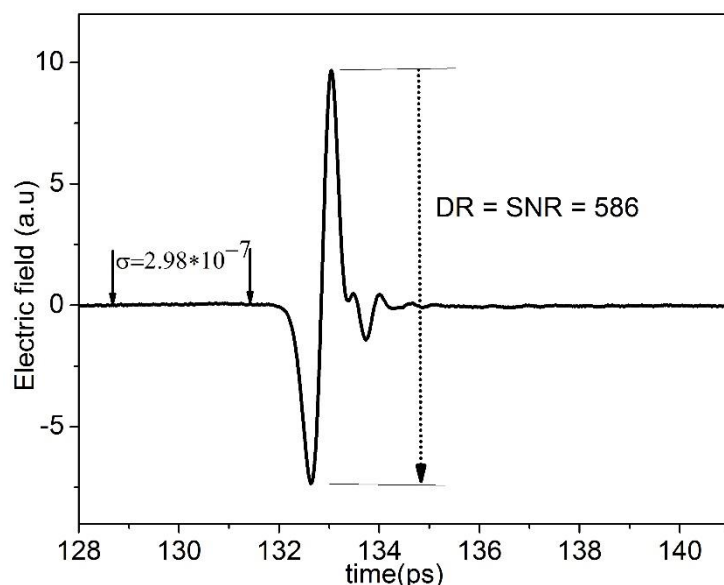


**Figure 15.** Average of 5 sequential time domain signals that is used for SNR calculation

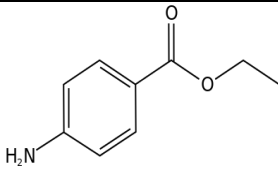
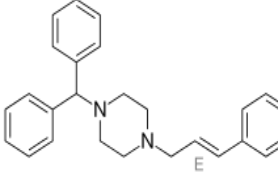
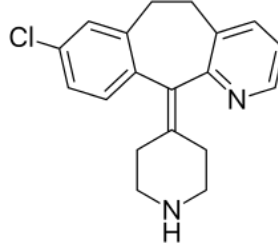
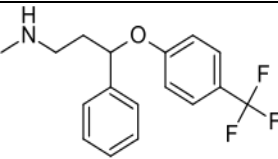
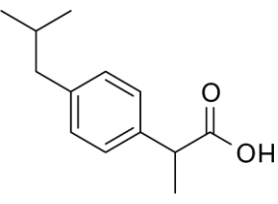
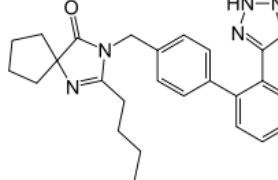
**Table 2.** SNR and DR of average of 5 sequential signals

Maximum magnitude of the amplitude	Standard deviation of the noise floor	DR
$17.5 \times 10^{-5}$	$2.98 \times 10^{-7}$	$5.86 \times 10^2$

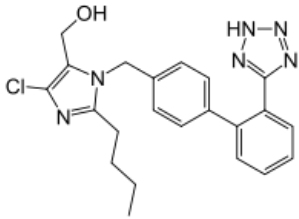
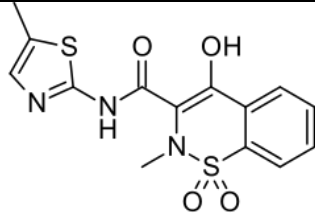
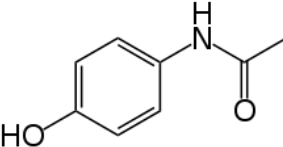
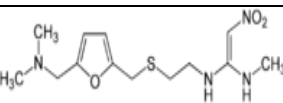
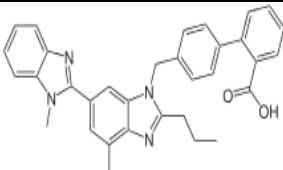
## 2.8 Sample preparation

Our analytes were API samples all of which was in powder form with fine particle sizes. The pure API were obtained as powder form from a commercial company, the commercial drugs of APIs were obtained from the pharmacy. The analytes have undergone no further purification. Our binder and diluent, Polyethylene (PE), obtained from Micro Powders Inc. which has mean particle size of 10  $\mu\text{m}$ . Moreover, the commercial tablets were obtained from pharmacy. Our analytes included the following;

**Table 3.** The list of APIs' name formula, and structure

Name	Formula	IUPAC name	Molecular structure
Benzocaine	C <sub>9</sub> H <sub>11</sub> NO <sub>2</sub>	Ethyl 4-aminobenzoate	
Cinnarizine	C <sub>26</sub> H <sub>28</sub> N <sub>2</sub>	(E)-1-(Diphenylmethyl)-4-(3-phenylprop-2-enyl)piperazine	
Desloratadine	C <sub>19</sub> H <sub>19</sub> ClN <sub>2</sub>	8-chloro-6,11-dihydro-11-(4-piperidinylidene)-5Hbenzo[5,6]cyclohepta[1,2-b]pyridine	
Fluoxetine HCl	C <sub>17</sub> H <sub>19</sub> ClF <sub>3</sub> NO	N-methyl-3-phenyl-3-[4-(trifluoromethyl)phenoxy]propan-1-amine	
Ibuprofen	C <sub>13</sub> H <sub>18</sub> O <sub>2</sub>	(RS)-2-(4-(2-Methylpropyl)phenyl)propanoic acid	
Irbesartan	C <sub>25</sub> H <sub>28</sub> N <sub>6</sub> O	2-butyl-3-({4-[2-(2H-1,2,3,4-tetrazol-5-yl)phenyl]phenyl)methyl)-1,3-diazaspiro[4.4]non-1-en-4-one	

**Table 3** continued

Losartan potassium	$C_{22}H_{23}ClN_6O$	(2-butyl-4-chloro-1-[[2'-(1H-tetrazol-5-yl)biphenyl-4-yl]methyl]-1H-imidazol-5-yl)methanol	
Meloxicam	$C_{14}H_{13}N_3O_4S_2$	4-hydroxy-2-methyl-N-(5-methyl-2-thiazolyl)-2H-1,2-benzothiazine-3-carboxamide-1,1-dioxide	
Paracetamol	$C_8H_9NO_2$	N-(4-hydroxyphenyl)acetamide	
Ranitidine HCl	$C_{13}H_{22}N_4O_3S$	(E)-1-N'-[2-[[5-[(dimethylamino)methyl]furan-2-yl]methylsulfanyl]ethyl]-1-N-methyl-2-nitroethene-1,1-diamine;hydrochloride	
Telmisartan	$C_{33}H_{30}N_4O_2$	2-[4-[[4-methyl-6-(1-methylbenzimidazol-2-yl)-2-propylbenzimidazol-1-yl]methyl]phenyl]benzoic acid	

Samples were analysed in pellet forms having 13 mm diameter. Pellet samples at various API concentrations were prepared as follows. The PE powder is mixed with API homogeneously. After the mixing process, 1 ton of pressure applied for 20 seconds to have a fine pellet. However, the pure pellets of APIs required more tonnage to form a pellet. They were obtained by applying over 5 tons of pressure for 5 mins under mild vacuum to ease the pellet making process. API samples were prepared in 5, 7.5 and 10 % w/w concentrations in PE.

In order to have a fine pellet, the powder size should be as small as possible. Most of our samples had particle sizes small enough but the other ones were needed to be grounded by the help of mortar and pestle. Furthermore, the pellet should have homogeneous thickness all around. This could be achieved by placing the sample powder inside the die, over the lower anvil. After placing it, the plunger of the die is used to gently pressing on the powder while rotating the plunger for some time for levelling. The pellets should have smooth surfaces in order to minimise scattering of radiation. Thus, both upper and lower anvils should have smooth, polished surfaces. Finally, the applied pressure during the pellet making is important. The pressure should be as low as possible to minimise the stress but should be high enough to achieve smooth surfaces. The way of releasing the pressure is also crucial. For example, if 10 tons of pressure is applied to a pellet, an abrupt release of pressure may cause shock effect on the pellet, which could disrupt the integrity of the pellet. Therefore, there should be a slow releasing rate of the pressure to avoid cracks that could be experienced by the pellet.



## CHAPTER 3

### SYSTEM SETUP AND OPTIMISATION STUDIES

One of the main purpose of the study presented throughout this thesis is setting up a THz-TDS system with the best possible SNR and DR as well as the bandwidth. Thus once each set-up is achieved, the system is optimised and then compared to each other. After a successful setup, the spectrometer was tested with materials whose properties presented in the literature. Once the best set-up is achieved, the final system is used in API studies.

Common equipment of each set-up are an ultrafast laser, THz generators and detectors, detector crystals, optics, translation stages, and other equipments necessary for data acquisition, like lock-in amplifier, data acquisition card and data acquisition software. At first, antenna generation-antenna detection system was tried. In this setup PCAs were employed for both THz generation and detection. This system has some basic advantages over antenna generation-crystal detection system. It is easier to setup the system because there are less number of optics: electrooptic crystal, quarter waveplate, Wollaston prism and balanced photodiode are not necessary thus it is cheaper. More importantly, PCA technique has generally better SNR reported ratio compared to crystal detection technique. The crystal has a certain thickness, resulting in multi-reflections of THz pulses from the interfaces of the crystals. These reflections may limit the bandwidth generated by the antenna and also limits the resolution of the spectra due to restricted windowing interval. Here the crystal thickness may be changed; however, there is a trade-off between bandwidth and SNR. As the crystal thickness increases, the SNR increases but due to the reflections and strong phonon modes of the crystal the bandwidth gets narrower. On the other hand, as the thickness

decreases, the bandwidth is extended with cost of lower SNR. However, these difficulties could be overcome with antenna generation and detection thanks to the technical improvements in this field. The antennae produced could have a bandwidth of as large as 30 THz [16]. Also, there is no reflection in the presence of antenna detection since the signal is directly measured as current by the help of a lock-in amplifier.

In the light of these facts, the setup studies were started with two antennae for generation and detection of THz radiation but it was continued with antenna generation crystal detection systems. The initial system included two antennae for both generation and detection. This system had low SNR therefore the detection system was changed with crystal detection with one OAPM.

### **3.1 System setups**

As briefly mentioned above, during our studies on setting up the system, we aimed to have best SNR. For this purpose, we have tried many different set-ups having different THz emitters and detectors to have as much signal and bandwidth as possible. The details are given in the following sections.

#### **3.1.1 Antenna-antenna setup**

Our first attempt to build the system was with two antennae for both emission and detection of THz radiation. The sketch of the system is given at **Figure 16**. Our initial plan was to check both antennae and then to add other optics (including OAPM's). Small diameter THz light, if possible, is preferred in our studies because it was among our plans to analyse our samples in terms of homogeneity.

To operate a PCA, there should be visible light focusing on the antenna gap and a bias voltage (for THz generation) or THz light (for detection) should be applied. The visible light should be as straight as possible to have ease on placing the antenna in the system. After placing the antenna, the light should be focusing on the antenna gap properly at recommended beam size and intensity by the producer company to produce high intensity and broadband THz radiation. To understand whether the light is focused on the gap properly, the antenna gap resistance is measured with a multimeter. A PCA

has certain gap resistance value when it is not illuminated since the used material is a semiconductor. This resistance decreases when the light hits on the antenna gap because the visible photons (or any photon which has more energy than the bandgap energy of the material) excites electrons to the conduction band of the semiconductor resulting in conditionally increased conductance of the material. The smaller the resistance, the better an antenna operates. Therefore, the antenna resistance should be lowered as much as possible by aligning position with the help of microstages.

We observed that the antennae, PCA and iPCA of models, had different resistances when they are not illuminated (dark resistance). Therefore, their response to illumination was different. The resistance of iPCA antenna could decrease from 32 k $\Omega$  to 0.3 k $\Omega$ . On the other hand, PCA antenna decreases from 5.4 M $\Omega$  to 0.7 M $\Omega$ . It was more difficult to decrease the resistance of PCA antenna because it has an optical lens attached to the front. This lens focuses the light onto 5 $\mu$ m antenna gap, making the proper alignment of the antenna more difficult. Once the resistances were decreased, the system was thought to be ready to see the signal; however, we obtained a very weak signal unexpectedly, resulting in very low SNR and narrow bandwidth. The time domain signal and corresponding frequency domain spectrum are given in **Figure 17**. To improve SNR, we changed the distance between the antennae ranging from 0-25 cm but none of them gave better result. Here both antennae were tried as generator and detector but there was really not much of an improvement. Communication with the supplier and eventually sending the antennae for control made no difference. Thus, we decided to switch the detection technique to EO sampling method.

**Table 4** Resistance of the antennae

	<b>Dark resistance</b>	<b>Illuminated resistance</b>
iPCA	32 k $\Omega$	0.3 k $\Omega$
PCA	5.4 M $\Omega$	0.7 M $\Omega$

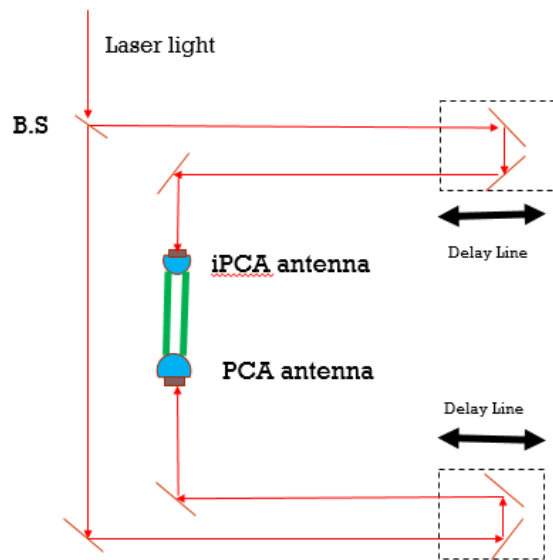


**Figure 16.** Antenna-antenna system setup

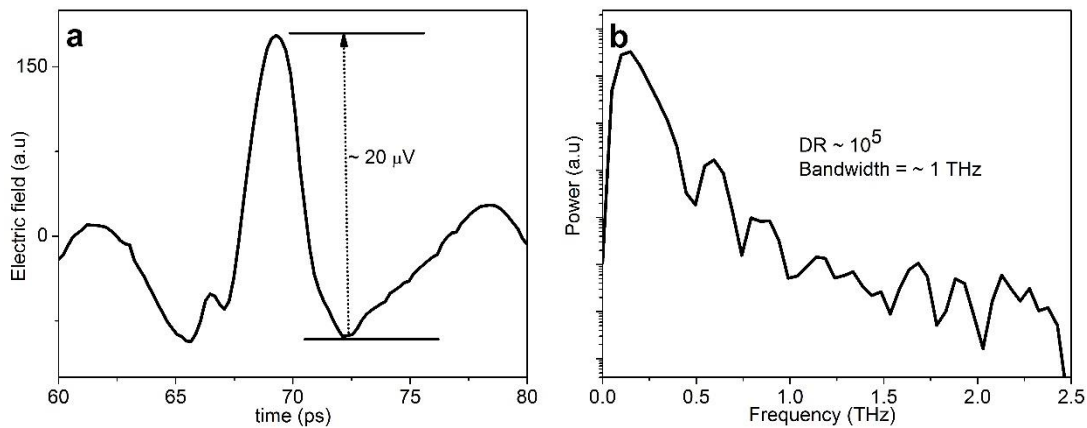


**Figure 17.** a) The signal obtained from the antenna-antenna system and b) its frequency components

### 3.1.2 Antenna-crystal set-up

In this type of configuration, additional optics and detectors are required compared to an antenna detection system, namely ZnTe crystal, Quarter waveplate, Wollaston prism and a balance photodiode. To shortly mention their usage purposes, ZnTe was used as nonlinear optical media with birefringent property causing polarisation change

of visible pulse. The Quarter waveplate was used to rotate the polarisation further and the Wollaston prism was used to split the laser beam according to its plane polarisation components. Finally, a balance photodiode was used to detect THz light by detecting the intensity change of the split light.

Normally three OAPMs are needed in this system to have a beam size comparable to sample size (13 mm) because the beam coming out of the antenna is almost 20 mm in diameter. However, the beam size should be smaller to be able to analyse the sample without losing signal intensity of the THz beam. For simplification, the system was set-up with just one OAPM (**Figure 18**). This was the first set-up would be simpler and step-wise. Since the THz beam coming out of the antenna is collimated by a Teflon lens attached to the antenna assembly, one OAPM was enough to have the light focusing onto the crystal. After seeing the components of the system working, a more complicated system is constructed.

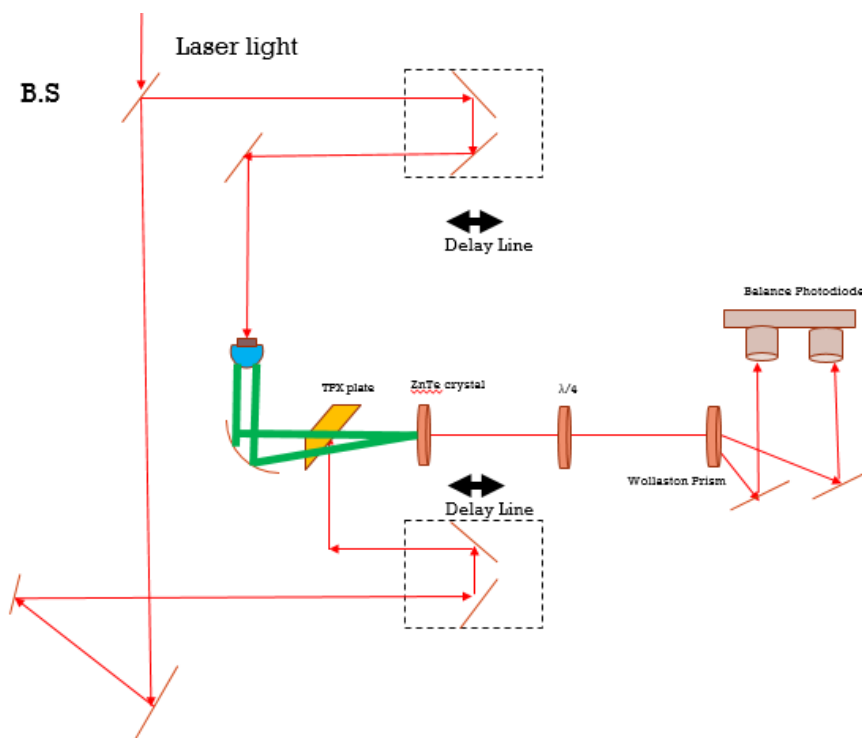


**Figure 18.** Antenna-crystal system setup with one OAPM

Once the optics and equipment are placed properly and aligned well the obtained signal was rather improved compared to antenna-antenna system. The bandwidth was extended to ca. 2.4 THz and DR was improved to ca.  $10^5$  as presented in **Figure 19**. Thus, it was decided to continue with antenna generation and crystal detection configuration to further improve the system.

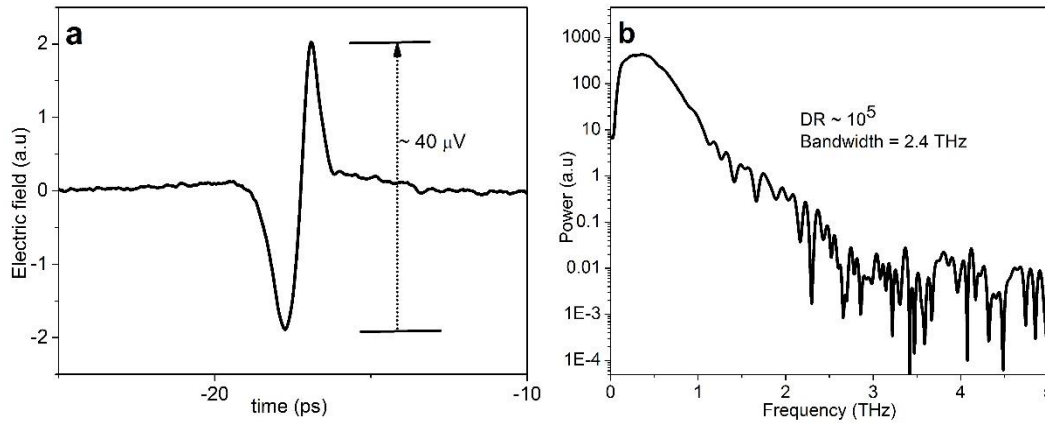


**Figure 19.** a) The signal obtained with Antenna-crystal system setup with one OAPM and b) its frequency components

The THz beam coming out of an antenna assembly (with Teflon lens) has a diameter around 20 mm. In order to reduce the beam size smaller than the aperture of our sample holder (13 mm), a different configuration was designed employing three OAPMs. In this set-up the first mirror is for focusing the beam onto the sample, the second one is for collimating and reducing the size and the third one is for focusing onto the ZnTe crystal (**Figure 20**). In this configuration, both iPCA and PCA antennae were tried for THz emission but we have not observed any signal with PCA antenna. Thus we decided to continue using iPCA antenna as our THz generator. This also showed that the PCA antenna is possibly the one that did not work properly in antenna-antenna configuration. After careful alignment and optimisation, we got the best signal with the highest SNR and bandwidth of 2.4 THz. Due to changes in ambient conditions like in humidity and the temperature, day-to-day operations and consistent measurements was difficult. This was minimised (less than 1% humidity) by having a dry air zone

along the THz beam path. Having dry air not only provides stable results but also cause the THz signal intensity to increase since the attenuation caused by water vapour is minimised. A purge box is built around the THz beam path. The resultant signal after having purged air is shown in **Figure 21**. However, the obtained SNR was lower than expected. After carefully inspecting the system, we have thought that the system could improve further if we remove the Teflon lens from the iPCA antenna since Teflon lens has low THz transparency compared to other polymers like HDPE, TPX, or reflective optics.

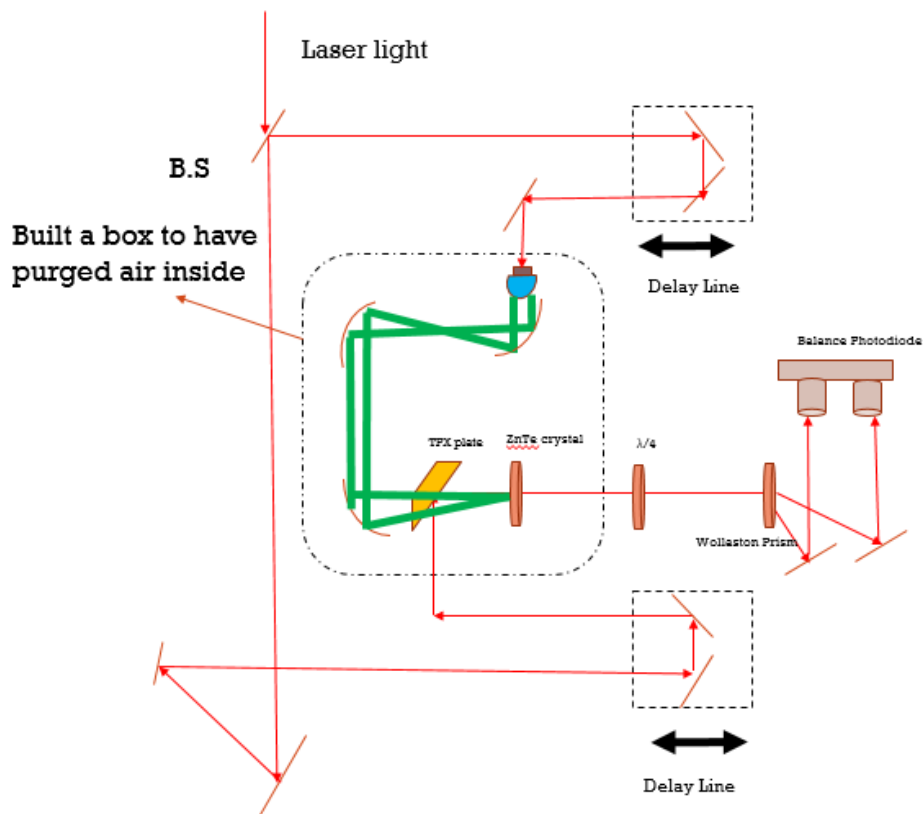


**Figure 20.** Antenna-crystal system purged with dry air (dash-dotted box)

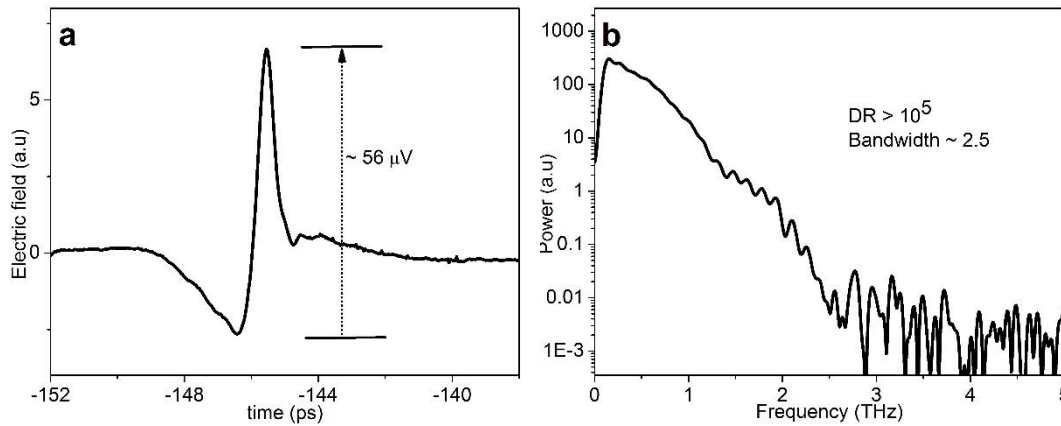


**Figure 21.** a) The signal obtained with three OAPM system and b) its frequency components

After removing the lens, the system was reorganised because the THz beam emitted from the antenna was not collimated. First, a simple system was set-up with two OAPMs because minimum two OAPMs are required to focus the beam onto the ZnTe crystal in order to see if the removal of the Teflon lens would result in any improvement (**Figure 22**). After setting up the system there was an apparent increase in both the THz field amplitude and our bandwidth, which resulted significant increase especially in high frequency side of the THz frequency profile. (**Figure 23**)

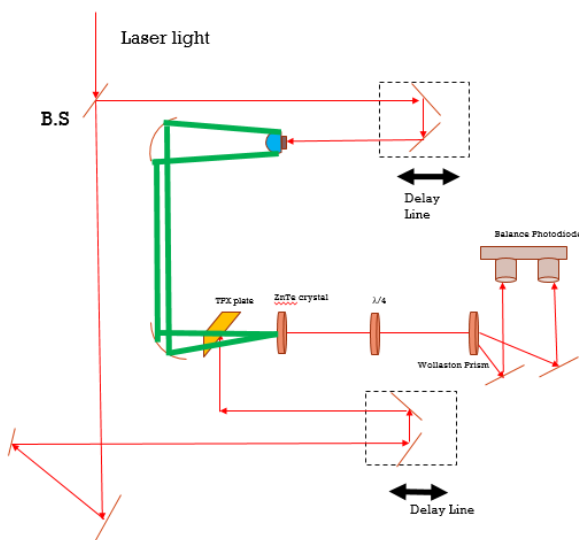


**Figure 22.** Antenna-crystal system with 2 OAPMs. The Teflon lens of the antenna is removed thus 2 OAPMS are needed to focus the light on the detection crystal

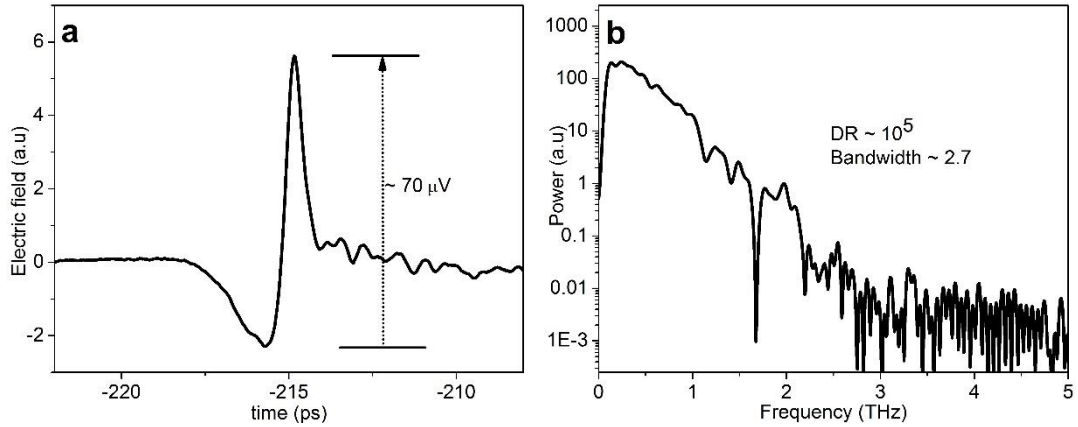


**Figure 23.** a) THz time domain signal and b) its frequency component obtained by the system

After this basis test and observation of apparent improvement of the THz signal, a new configuration was designed. As the next step, an 8F OAPM system was built (**Figure 24**) and optimisations were made which resulted in the final version of the spectrometer. A clear improvement can be seen at **Figure 25**. As a result, ca 3 THz bandwidth, SNR > 10<sup>5</sup> and beam size of <13 mm were successfully achieved. (**Figure 25**).

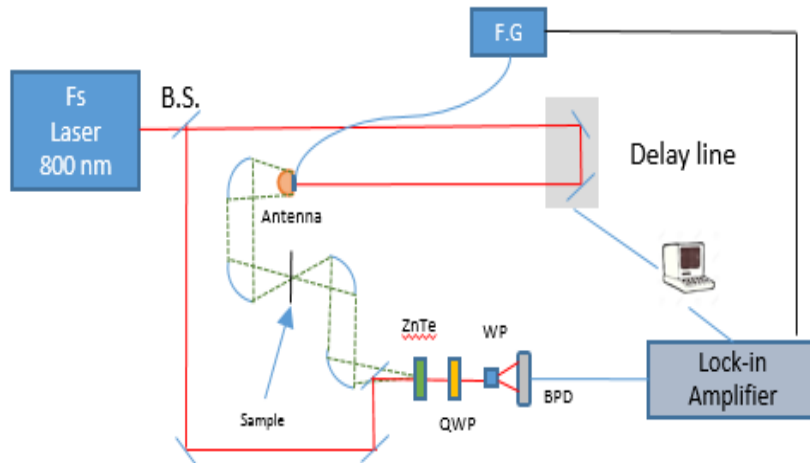


**Figure 24.** Final version of the system; 8-F OAPM system

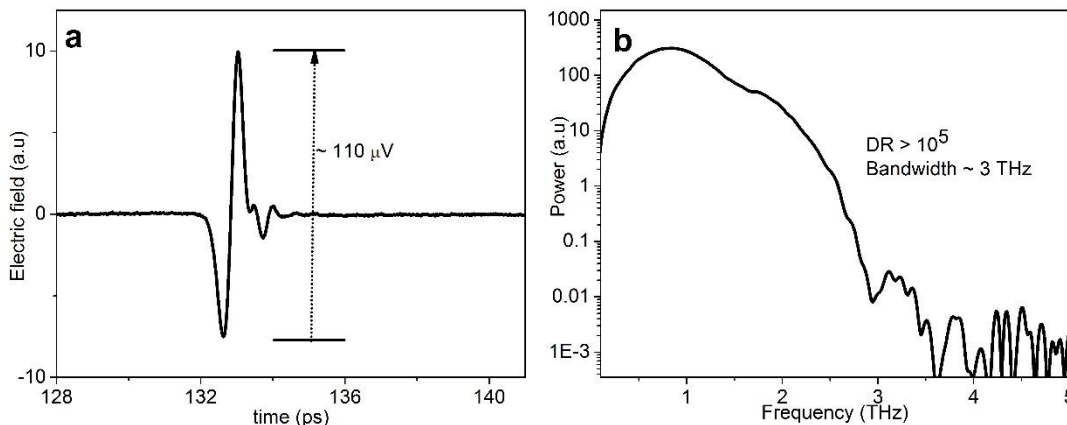


**Figure 25.** a) Time and b) frequency domain profiles of THz field obtained by the final 8F configuration of the system.

- **System test**

After having optimised system, a sample whose literature study was already available was analysed and presented in **Figure 26**. The sample was Ibuprofen, which is commercially available. King et al. reported in literature by a sample spectrum at both room and liquid nitrogen temperatures. [5] The reported Ibuprofen has spectral features located at  $35.8 \text{ cm}^{-1}$ ,  $51.2 \text{ cm}^{-1}$ ,  $64.1 \text{ cm}^{-1}$  and  $84.5 \text{ cm}^{-1}$  at room temperature. The first band is relatively intense and well resolved whereas the second one is broad and weak. The third is also broad and fairly strong. The fourth band is broad and weak as well. These very bands were also observed with our system at the same wavenumbers. However, the relative intensity of our bands were lower because we had the sample pellet with 12% but lower total mass; 100 mg. In addition, we have observed a stronger scattering possibly due to use of different PE filling material.

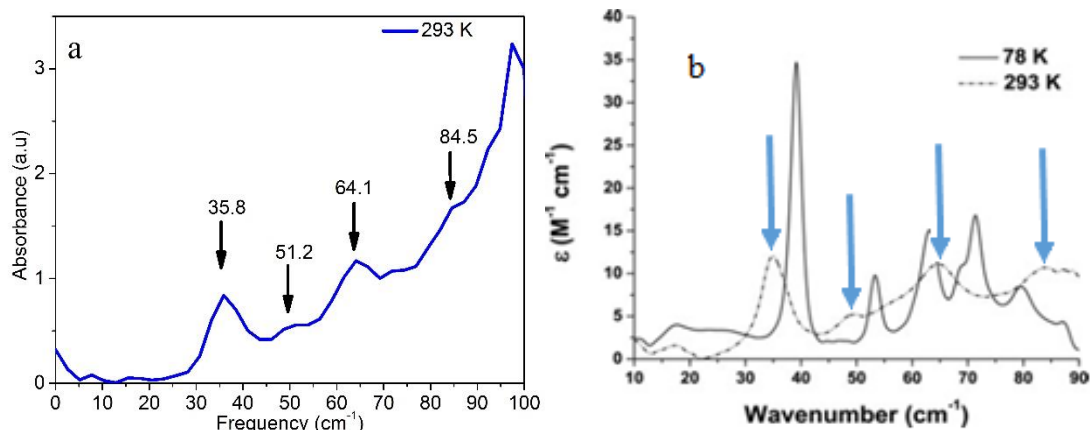


**Figure 26.** Ibuprofen spectra a) collected with our system and b) available in the literature[5]. The literature result belongs to (RS) ibuprofen which was analysed at both 78 and 293 K.

### 3.2 Sample angle effect

If the sample is in solid state and it is analysed in pellet form, the incidence angle of the light to the sample could be important. For instance, when there is a thin pellet, the pulses would cause multiple reflections from the interfaces. This results in fringes on the frequency data after Fourier transformation. To eliminate this, time domain data needs to be cleaned from those reflections. This not only limits the frequency range but also affect the observed bands. One way to determine the reflections in time domain data is by increasing the sample thickness. A simple way to increase the thickness while keeping all constant is tilting. Thus, in this part of the study the effect of tilting angle on the THz spectra were investigated. Here, only the angle perpendicular to propagation direction of THz light was changed. Initially, the sample was rotated ca. 20 degree and there was almost no change as could be seen in **Figure 27a**. Afterwards, the sample was rotated to have ca. 45 degree. There occurred a change which may be due to reduced THz beam size. Thus it is better to have a THz beam size smaller than the holder aperture. Generally, the beam comes with normal angle to the surface of the pellet. However, as the angle between the normal of the holder and the light propagation direction increases effectively sample aperture becomes smaller. As a result, only some portion of the beam would pass through the

holder depending the angle of rotation, as in the case of  $45^\circ$ . This loss in THz field is clear in the frequency domain (**Figure 27b**). However, a few degree of misplacement of the sample does not pose any problem.

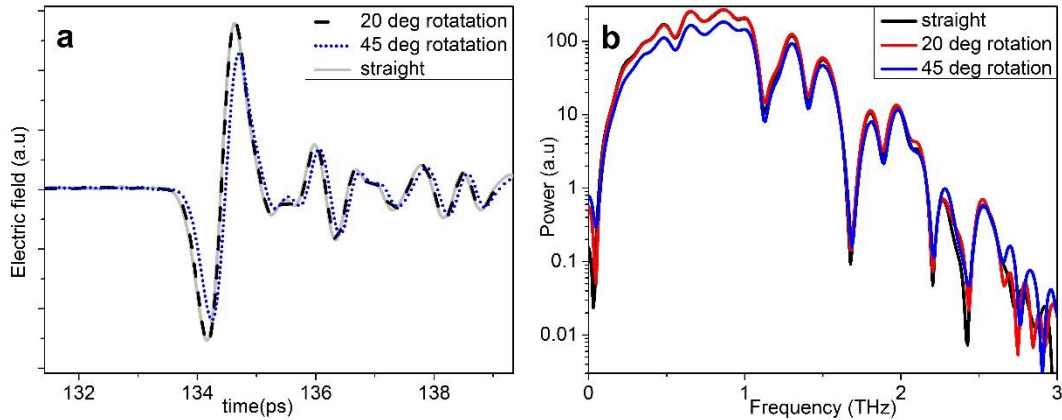


**Figure 27.** a) Sample rotation experiment with angles of ca. 0, 20 and 45 degrees b) FFT results of the rotation of sample experiment

### 3.3 Optimisation studies.

After obtaining the most promising system, it was optimised for sample measurements. In this part of the study, basic parameters of the set-up were checked and optimised. These are its stage speed, lock-in amplifier settings, and the controlling the atmosphere in the THz beam path.

#### 3.3.1 Scan mode and stage speed optimisations

Speed of a translational stage is important because it determines the resolution of the time domain signal obtained. This in turn determines the bandwidth in the frequency domain. In addition, if the stage does not scan slow enough, full profile of the signal may not be obtained, thus less intense signal than the actual signal could be observed. As a result, since the whole signal is not reached, the obtainable bandwidth gets narrower. Therefore, the aim here was to find the optimum stage speed in order to obtain the full shape of THz profile. For this purpose, various speed settings of

translational stage in different scanning modes; continuous and step scanning modes, were tried.

### 3.3.1.1 Continuous Scan Mode

In continuous scanning mode, the translational stage of the optical set-up travels from the initial set position to final set position continuously with certain set speed without stopping. The initial acceleration and final deceleration is set and constant. The stage speed is determined by the number of points setting in the Labview code and the time constant settings of the lock-in amplifier. The desired interval to be scanned by the stage generally consists of several picoseconds.

As presented in **Figure 28**, the stage speeds of 40, 50, 60 and 70 points per ps (pps) were tried initially. As the number of points increased a better profile of signal was obtained and the bandwidth became wider as the stage speed slowed down. Since the bandwidth is increased with decreasing stage speed, the speed was reduced further. At this stage, 80, 100, 120 and 150 pps were chosen as the stage speed in 13 ps window. In order to observe the effect more clearly, the measurements were done with a sample, Losartan potassium (5% w/w, in HDPE). This way it would be possible to observe the best resolved spectral features and compare to FT-THz spectrum of Losartan potassium.

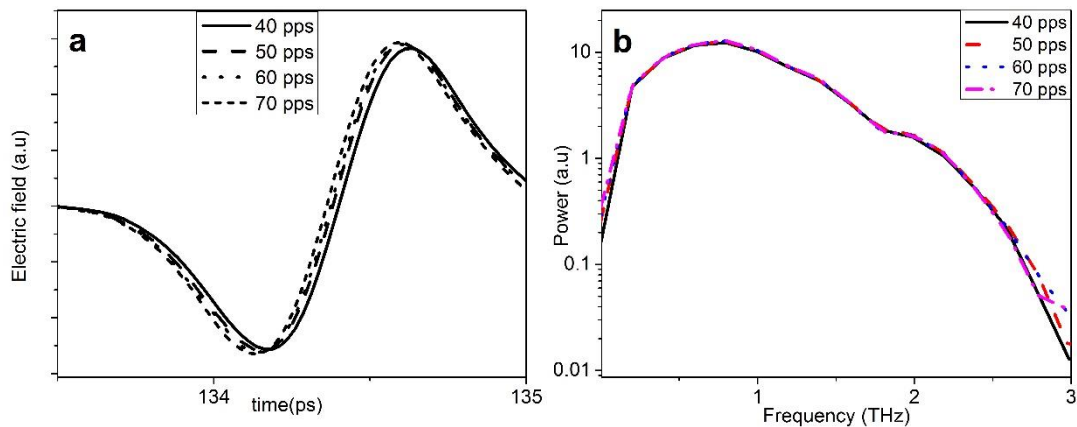


**Figure 28.** a) Signal profiles and b) bandwidth of different stage speeds (40 pps solid line, 50pps dashed line, 60pps dotted line and 70 pps dash-dotted line)

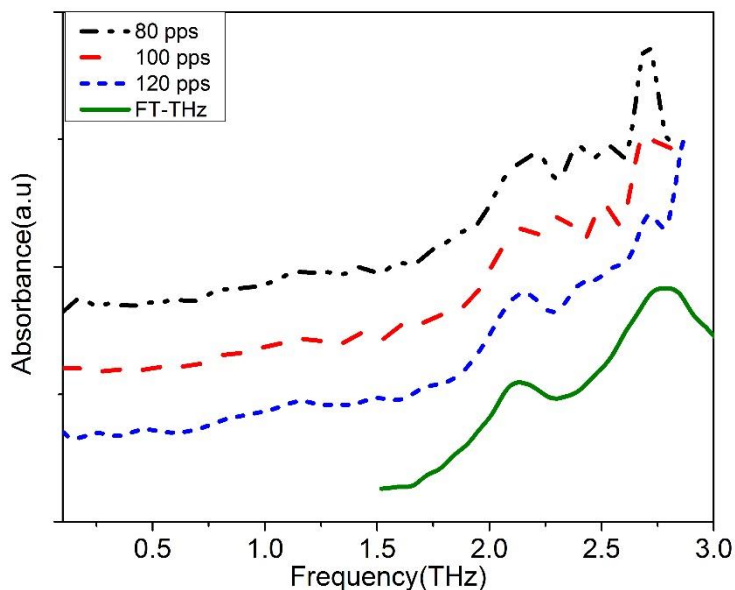


**Figure 29.** Absorption spectra of Losartan potassium collected at different stage speeds by THz-TDS and FT-THz systems. The spectra are shifted for clarity.

**The Figure 29** presents the result of absorption spectra of Losartan potassium obtained at different stage speeds. Each spectrum was obtained by having the average of repeated three measurements at each speed and lock-in amplifier had time constant setting of 100 ms for each measurement. The results showed as the number of points increased, the obtained spectrum became smoother and similar to the FT-THz spectrum of the same sample.

### 3.3.1.2 Step scan

Another possible mode for data collection is step scanning mode. In this mode, the stage moves in steps with certain step sizes and it stops for a predetermined time to collect data at each step point. This results in better SNR because it could allocate more time for data collection. However, there is a trade-off in step scan mode. As the data acquisition time increases for better SNR, the reliability of the data may decrease because of the instabilities of the ambient conditions present in the laboratory. The total time duration of one measurement could last for hours. For example, data collection with 1  $\mu\text{m}$  step size and 600 ms waiting time lasted 45 minutes, which is

quite long duration as compared to one scan in continuous mode with similar SNR (~3 minutes)

The sizes of the stage were 1  $\mu\text{m}$ , 3  $\mu\text{m}$ , and 6  $\mu\text{m}$  during the measurements and the waiting time after each step before data collection starts was 600 ms. The resulting spectra showed that the signal profile gets better as the step size decreased as shown in **Figure 30**.

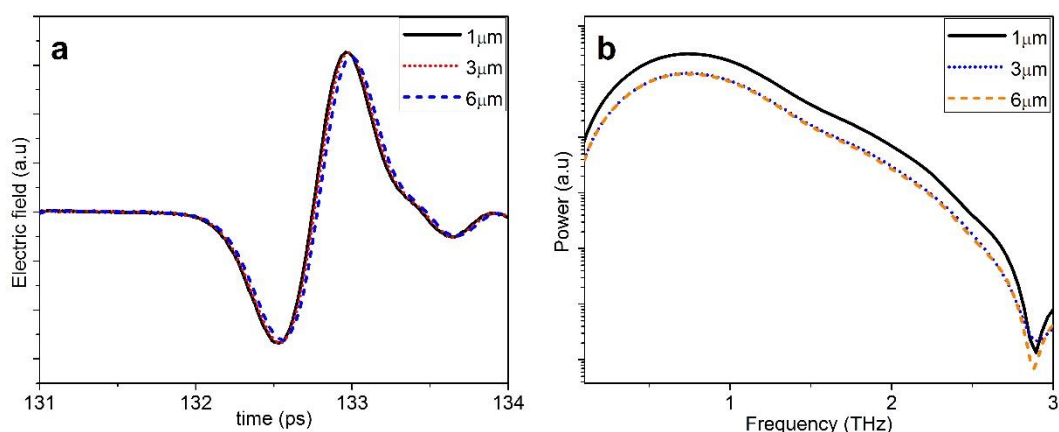


**Figure 30.** a) Signal profiles and b) bandwidth of different stage step sizes (1  $\mu\text{m}$  solid line, 3  $\mu\text{m}$  dotted line and 6  $\mu\text{m}$  dashed line)

#### - Step vs cont scan

To determine the best scanning mode, various stage speeds of step and continuous modes were compared. For the comparison, sample pellet of Losartan potassium was chosen. The sample was analysed with both THz-TDS and FT-THz systems and the result is presented (**Figure 31**). As presented in the **Figure 31**, step scan gave the best result with its 1 and 5  $\mu\text{m}$  step sizes whose spectra are close to the spectrum obtained by FT-THz. On the other hand, continuous mode with 150 pps is much better and looks more alike FT-THz result. Continuous mode is more advantageous because it requires shorter scanning time as compared to the step scanning mode. A scan of 13 ps window in continuous mode with 150 pps requires 195 seconds whereas the same window

interval requires 45 minutes in step mode with 1  $\mu\text{m}$  step size. Thus averaging the results of multiple scans of 150 pps gives the best spectra in much shorter time.

The scan length and scanning speed affect a spectrum. The scan length determines the frequency resolution whereas the scan speed influences the achievable bandwidth. These parameters are calculated for our system by using the following formulas;

$$\text{Freq. res.} = \frac{1}{\Delta t} = \frac{1}{13 \text{ ps}} = 76.9 \text{ GHz} \quad 7$$

$$\text{Achievable bandwidth} = \left(\frac{n}{\Delta t}\right) = \frac{1950}{13 \text{ ps}} = 150 \text{ THz} \quad 8$$

where ' $\Delta t$ ' is the time windowing of the scan and n is the number of points of the scan

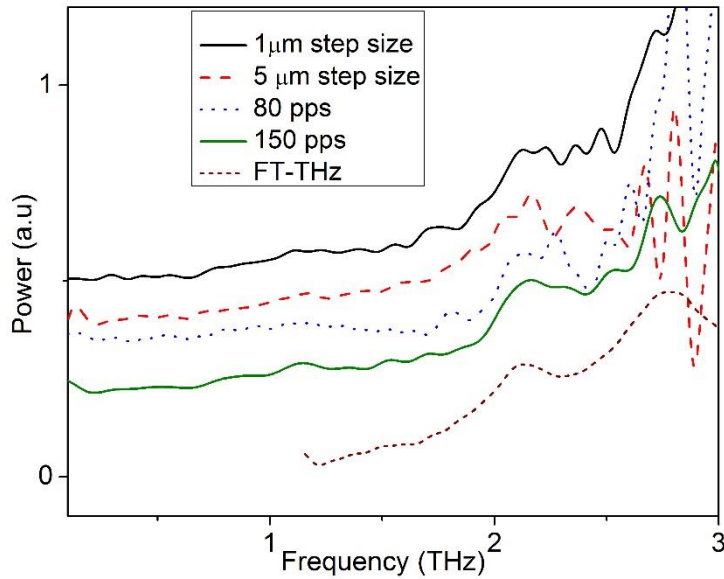


**Figure 31.** Comparison of step and continuous modes with different stage speeds

### 3.3.2 Lock in parameters optimisation

Lock-in parameters are also significant since they directly affect the SNR. In order to find the optimum results, all of the settings of lock-in amplifier checked for the best SNR.

#### 3.3.2.1 Signal input settings (AC coupled, DC coupled, Float)

These settings did not have considerable difference in their time domain spectra as could be seen from the **Figure 32** and **Table 5**, thus we have chosen DC coupled setting since it had the lowest standard deviation.

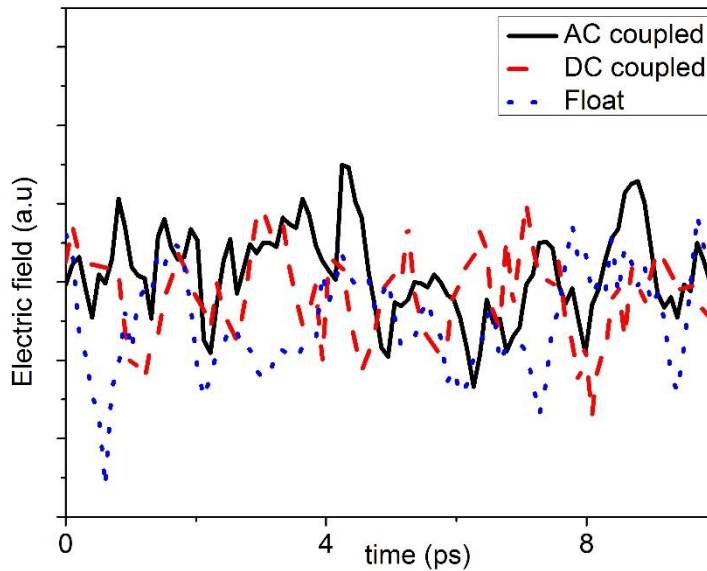


**Figure 32.** Time profile collected with AC coupled, DC coupled and Float settings of lock-in amplifier.

**Table 5.** Mean and standard deviation of data given in **Figure 32**

Setting	Mean	Standard Deviation
AC coupled	$2.32 \times 10^{-8}$	$1.15 \times 10^{-7}$
DC coupled	$-3.21 \times 10^{-8}$	$1.11 \times 10^{-7}$
Float	$-9.79 \times 10^{-8}$	$1.29 \times 10^{-7}$

### 3.3.2.2 Sensitivity setting

Sensitivity of the lock-in is also an important parameter that especially affects the noise level. Here, all sensitivity scales have been tested. There appears some random noise as the sensitivity becomes larger than the maximum signal level (**Figure 33a**). The bandwidth is also affected from the sensitivity setting. The bandwidth becomes the largest when the sensitivity setting is  $500\ \mu\text{V}$  (**Figure 33b**).

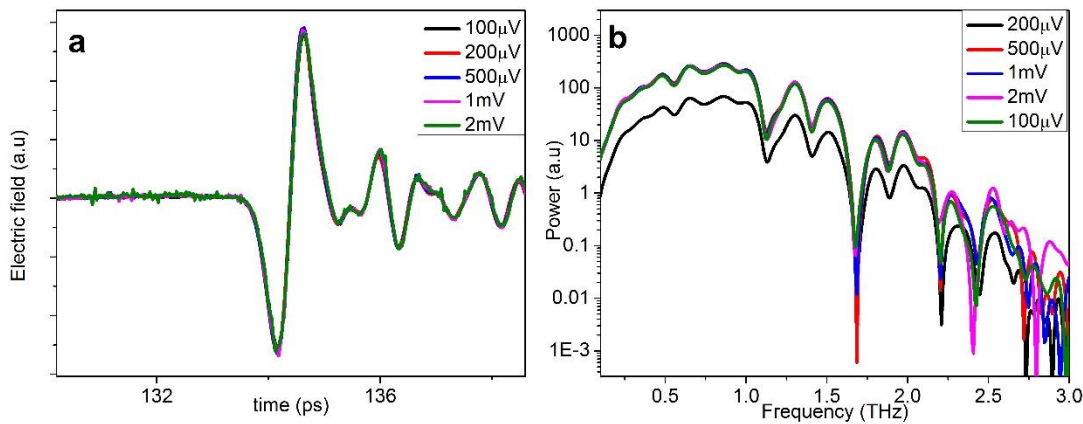


**Figure 33.** a) Time domain profile with several sensitivity settings of lock-in b) FFT of the signals given in a.

### 3.3.2.3 Reserve settings of lock-in

These settings did not result any difference in time domain profiles. (**Figure 34**, **Table 6**) The high reserve had slightly higher noise. ‘Normal’ setting was chosen since it had the lowest standard deviation.

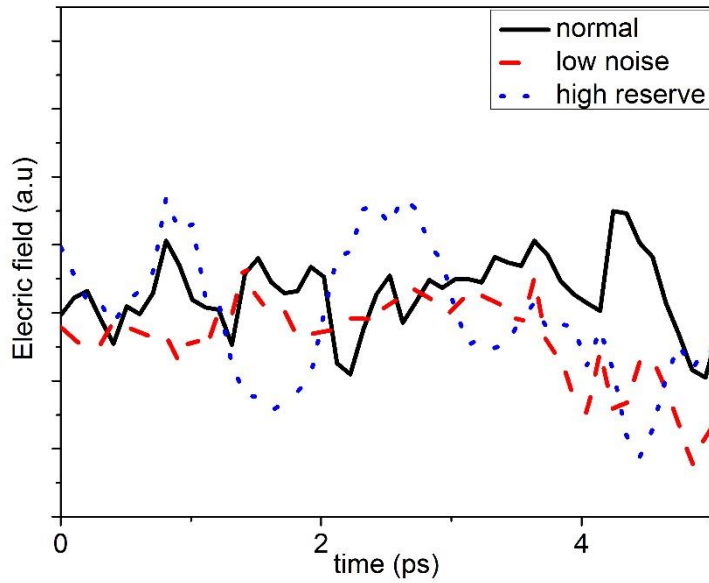


**Figure 34.** Time profiles at 3 different reserve settings of lock-in

**Table 6.** Mean and standard deviations of the signals obtained with the different reserve settings

Setting	Mean	Standard Deviation
Normal	$2.32 \times 10^{-8}$	$1.15 \times 10^{-7}$
Low noise	$-6.08 \times 10^{-8}$	$1.22 \times 10^{-7}$
High Reserve	$5.03 \times 10^{-8}$	$2.32 \times 10^{-7}$

### 3.3.2.4 Time constant dB settings

No significant difference was observed while changing the dB setting of the lock-in. (**Figure 35, Table 7**) The setting with the lowest standard deviation, 24 dB, was chosen.

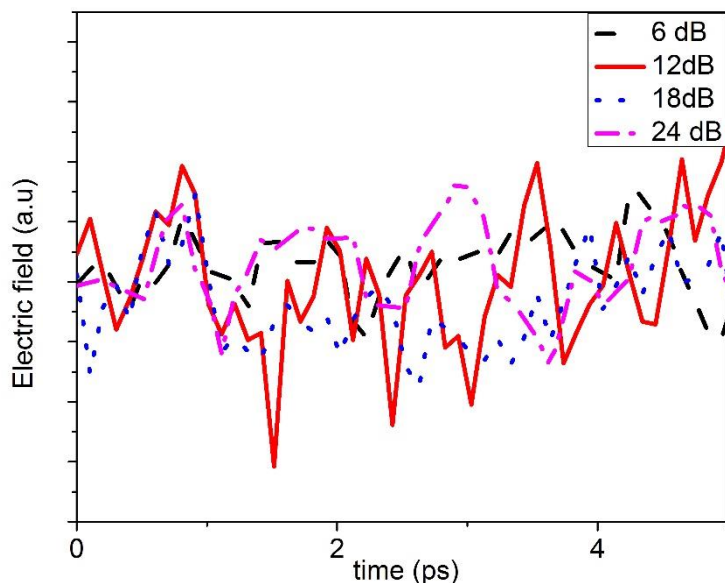


**Figure 35.** Time constant dB settings of lock-in

**Table 7.** Mean and standard deviations of the time constant dB settings shown in **Figure 35**

Setting	Mean	Standard Deviation
6dB	$-7.94 \times 10^{-9}$	$2.39 \times 10^{-7}$
12dB	$-7.41 \times 10^{-8}$	$1.41 \times 10^{-7}$
18dB	$2.59 \times 10^{-8}$	$1.48 \times 10^{-7}$
24 dB	$2.32 \times 10^{-8}$	$1.15 \times 10^{-7}$

### 3.3.2.5 Time constant

Time constant is an important parameter because it determines the time required for each measurement of a sample. If the system is not stable enough, longer duration of measurements could decrease the SNR due to the fluctuations in the system.

The first test with the time constant setting was done in continuous mode. Firstly, the measurements were taken with only noise floor. Then a sample of API, Losartan potassium, was analysed to see the effect on the bandwidth. Then in the second part,

the mode of the stage was switched to step scan and the effect of time constant was investigated and compared to the continuous scan.

Time constant settings and noise level have an inverse proportionality. That is as the time constant increases the noise decreases as **Figure 36** and **Table 8** presents. Also the effect of averaging was investigated. Noise floor scanned for 10 times with 100 ms time constant, 3 times with 300 ms time constant, and 1 time with 1 s time constant. The multiple scans were averaged to be compared and the result is presented in **Figure 37**. The results showed that there is no considerable difference in standard deviation between 1s, 3x300ms or 10x100ms data collection. (**Table 9**) In addition, the effect of averaging was monitored on bandwidth. The sample of losartan potassium was scanned for 3 times with 100 ms time constant and once with 300 ms time constant. The results were compared to the FT-THz spectrum of the same sample as presented in **Figure 38**. The Figure demonstrates that there appears to be not much of a difference between the two.

**Table 8.**Mean and standard deviation of noise level obtained with different time constant settings

<b>Setting</b>	<b>Mean</b>	<b>Standard Deviation</b>
100ms	-2.49x10 <sup>-8</sup>	1.89x10 <sup>-7</sup>
300ms	2.35x10 <sup>-8</sup>	1.16x10 <sup>-7</sup>
1s	-1.79x10 <sup>-8</sup>	8.73x10 <sup>-8</sup>
3s	-1.22x10 <sup>-8</sup>	7.87x10 <sup>-8</sup>

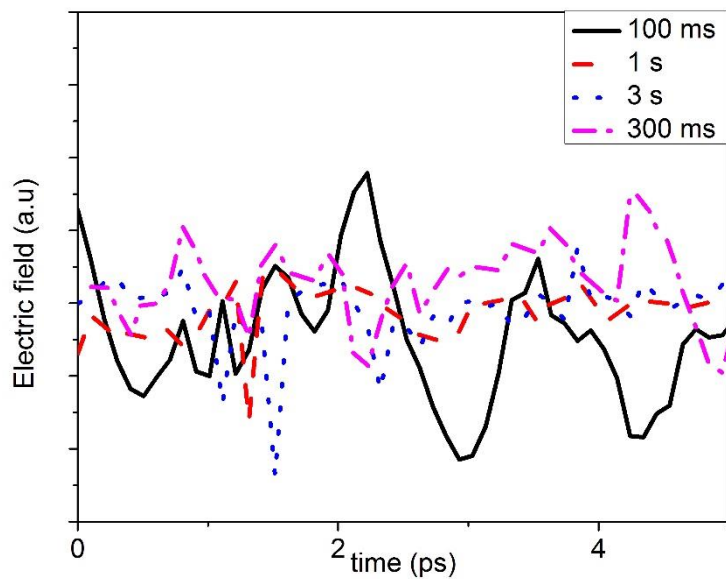


**Figure 36.** Signal of the noise floor obtained with different time constants

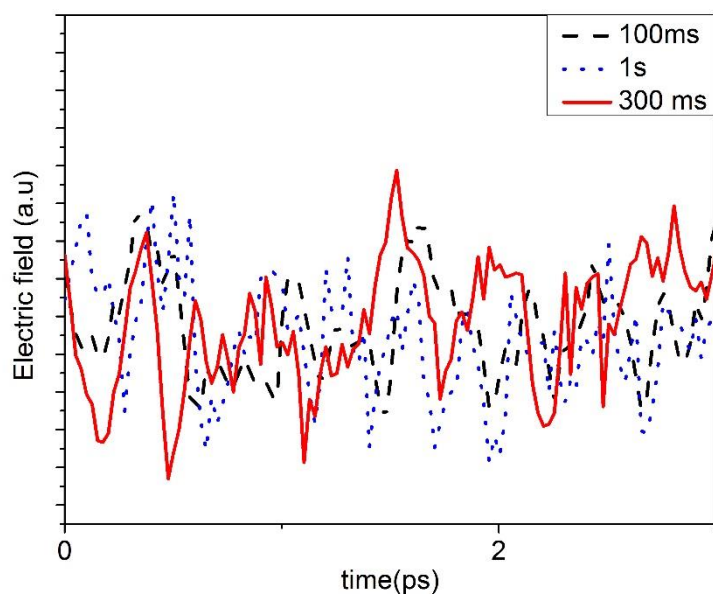


**Figure 37.** Effect of averaging on results with 100, 300 ms and 1 s time constants

**Table 9.** Mean and standard deviation of the noise level with 100 ms, 300 ms and 1 s time constants

Setting	Mean	Standard Deviation
average of 10x100 ms	$-1.11 \times 10^{-8}$	$7.05 \times 10^{-8}$
1 s	$-9.73 \times 10^{-9}$	$7.91 \times 10^{-8}$
Average of 3x300 ms	$-1.89 \times 10^{-8}$	$7.74 \times 10^{-8}$

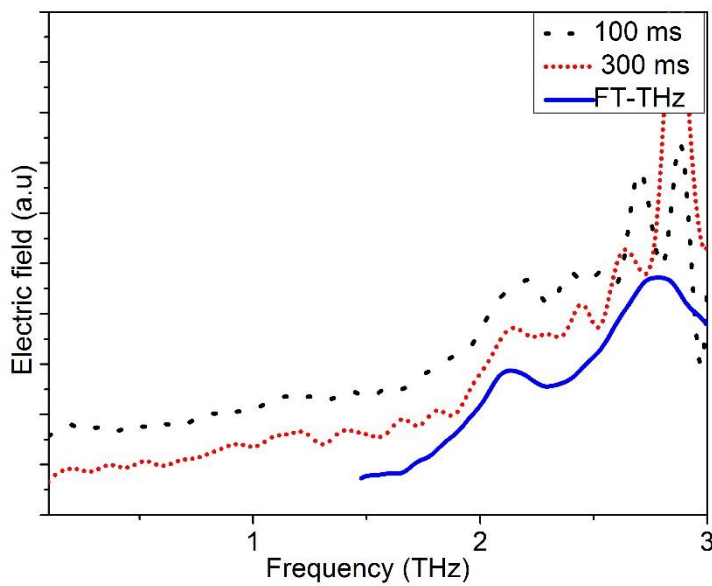


**Figure 38.** The effect of time constant on the achievable bandwidth of Losartan potassium. The speed of the stage was equal or each of 100 ms and 300 ms time constants (80pps)

### 3.3.3 Stage hysteresis problem

Back to back multiple scans of the same interval showed that the maximum amplitude of transient profiles did not have the same position due to either an error in the Labview code or a reproducibility error of the stage itself. In order to identify the source, following series of experiments were performed:

- i. Normal scan
- ii. Starting scanning from left side of the initial scanning point
- iii. Scanning by bringing the stage to its initial position manually

These tests were performed both in continuous and step scan modes.

### 3.3.3.1 Continuous scan

#### 3.3.3.1.1 Auto initial point

When the scanning is complete, the stage stays in the final point of the scan. Afterwards, when there is another command to have another scan, the stage goes to the initial point itself and starts scanning. The following plot belongs to this type of auto initial point scanning. As can be seen in **Figure 39a**, there is considerable shift (**0.0316 ps**) in the position of the THz pulse after the scans.

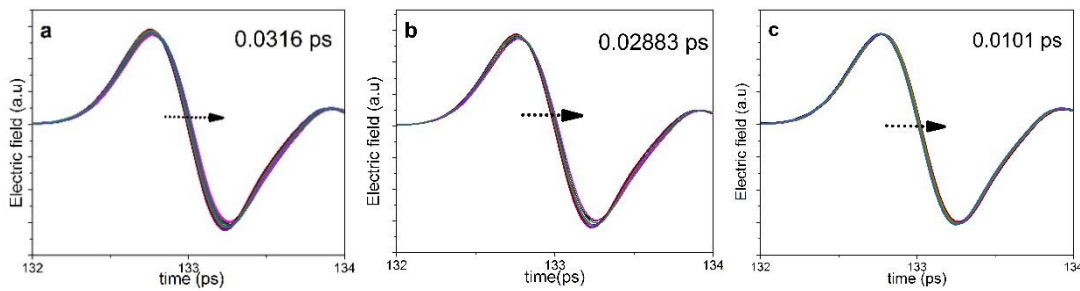


**Figure 39.** a) Multiple scans of normal scanning mode without any outside intervention. b) Bringing the stage manually to a position that is on the left hand side of the initial point. The stage normally comes to the initial point from the right hand side. c) Manual positioning of the stage to the initial position of the scan

#### 3.3.3.1.2 Manual positioning of initial point from the left hand side

It was thought that there could be mistake in codes of the Labview program thus the stage was not reaching to the initial point. Therefore, this time the stage was brought to a position which is on the left hand side of the initial point to see whether there would be a difference. The result showed that the shifting of the stage did not change considerably and it was **0.02883 ps (Figure 39b)**. This would mean that the stage was not able to come to the initial point reproducibly, which may be due to the software that we use, or acceleration, and/or deceleration settings etc. of the stage motors.

### 3.3.3.1.3 Manual positioning of initial point

Finally, the stage was positioned manually to the initial position of the scan. The results showed that shifting decreased to **0.0101 ps** (**Figure 39c**). This showed that the stage should be set manually to the initial point before a sensitive scan.

### 3.3.3.2 Step scan

After checking stage position reproducibility by continuous scanning mode, we also checked the reproducibility of the stage in step scanning mode.

#### 3.3.3.2.1 Auto initial point

Initially the stage was allowed to scan as controlled with the code to see the shifting amount in step scanning mode. The result showed that there was **0.0098 ps** shift, which is approximately the same as the value obtained with manual positioned stage in continuous scanning mode. (**Figure 40a**)

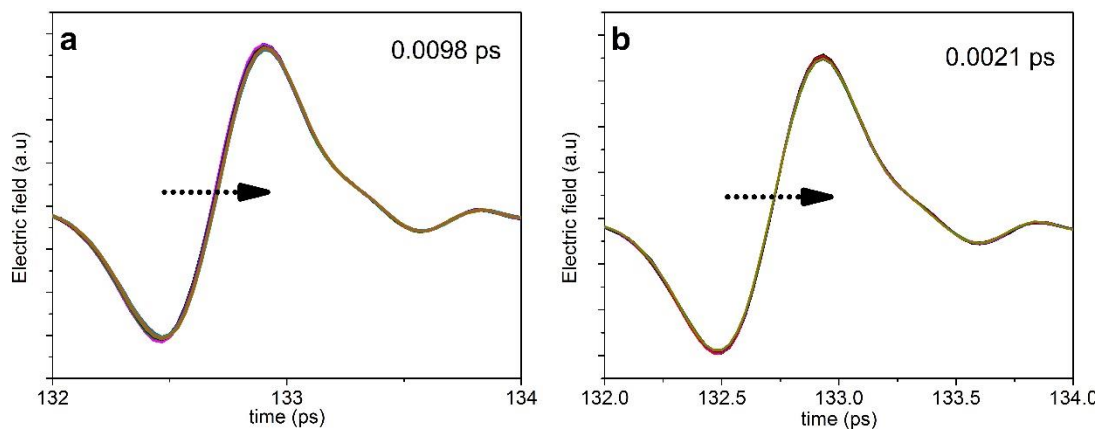


**Figure 40.** a) Normal scan in step scanning mode. b) Manual initial positioning of stage in step mode

#### 3.3.3.2.2 Manual initial point

After auto-initiation, manual positioning to the initial point was seen. As shown in **Figure 40b** the results of manual initial point of stage in step mode. The shift observed (**0.0021 ps**) was the minimum shift obtained so far in all modes and experimental conditions.

### 3.4 Dry Air Purged Box

The water vapour has strong attenuation of THz radiation. Thus elimination of water vapour as much as possible improves the background signal level thus improves SNR. In addition, the elimination of the water bands from the frequency domain spectrum resulted in increase in the bandwidth. The water vapour attenuation of THz signal is shown in **Figure 41**. Water vapour has strong rotational and vibrational transitions in the THz region. These absorption modes become significant as the frequency gets closer to 3 THz. After the elimination of water vapour, the achievable bandwidth extends to ca. 3 THz.

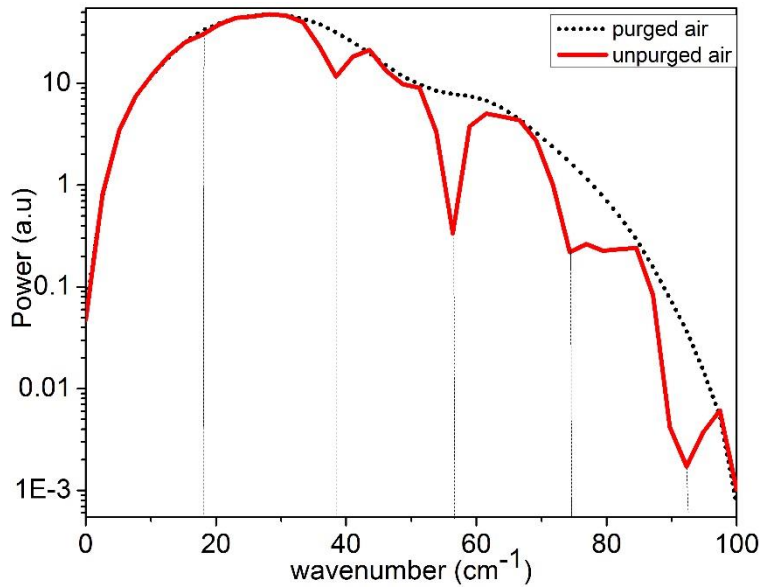


**Figure 41.** Bandwidth change before and after having dry air in the system. The strong water vapour bands present at 39 and 57  $\text{cm}^{-1}$  and the relatively weak band at 18  $\text{cm}^{-1}$  totally disappears.

### 3.5 Optimised System Parameters

After optimisation studies the following parameters are determined to give the best results and these parameters are used throughout our studies as presented in **Table 10**.

**Table 10.** Optimised system parameters

<b>Scanning mode of trans. stage</b>		Continuous scan	
<b>Length of scan</b>		13 ps	
<b>Number of points</b>		1950 (150 pps)	
<b>Lock-in Settings</b>	<b>Signal input</b>	DC coupled	
	<b>Sensitivity</b>	100 $\mu$ V	
	<b>Reserve</b>	Normal	
	<b>Time constant dB</b>	24 dB	
	<b>Time constant</b>	100 ms	
<b>Solution to stage hysteresis problem</b>		Bringing the stage to its initial position manually form left hand side	
<b>Data collection</b>		Measuring sample and its reference at least three times and averaging the results	
<b>Opt. Pow.</b>	<b>Generation arm</b>	3 mW (5 %)	
	<b>Detection arm</b>	500 mW (95 %)	
<b>Func. Gen.</b>	<b>Voltage</b>	14 V	
	<b>Frequency</b>	8 kHz	
<b>Laser</b>	<b>Wavelength</b>	CW	803 nm
		Modelocked	827 nm
	<b>Bandwidth</b>	CW	8 nm
		Modelocked	110 nm
<b>Pulse width</b>	Modelocked	80 fs	
<b>Angles</b>	<b>ZnTe crystal</b>		287°
	<b>Quarter waveplate</b>		100°
	<b>Wollaston prism</b>		55°



## CHAPTER 4

### RESULTS AND DISCUSSION

After successful setting up and optimisation of the system as mentioned in the previous chapter, the THz-TDS system was ready for the measurement of samples. Drug analysis is a new application area for THz spectroscopy. Even though optical properties of API have been widely investigated both in IR and visible regions, there are few studies in terahertz frequencies. With its many advantages THz spectroscopy brings new information and possibilities in drug analysis. The development of a THz technique for drug analysis would bring unique advantages to in-line, on-line and in situ analysis of drugs. Since the spectra of each API is unique to itself, these spectra would be used as fingerprints for detection and identification of APIs by THz technique. Thus, collection of spectra of APIs in THz region is necessary for future application of THz spectroscopy in drug analysis.

The most common dosage form is the tablet form. Therefore, all the measurements here concentrated on solid sample measurements. Our samples were in powder form, which also brought convenience for sample preparation as they were in pellet form. The pellet samples could be prepared from totally pure form or from a mixture with binder and excipient. The binder and diluent was usually chosen from materials with high transparency in THz region. Among them, polymethylpentene and high density polyethylene are the two most commonly used ones. The spectra of the two are given in **Figure 42**. Both of them show high transparency in THz region (~90%). Thus, they are preferred as filters, beam splitters, or sample holders for THz experiments.

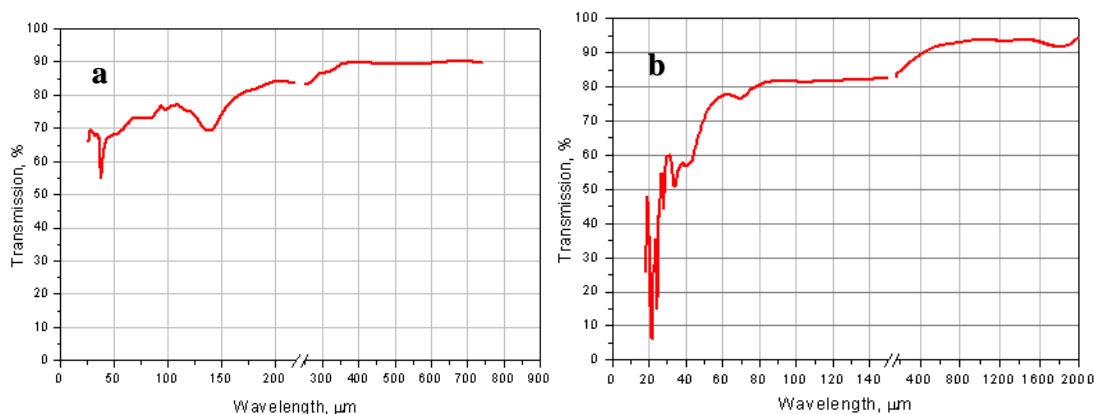


**Figure 42.** THz transparencies of a) polymethylpentene (TPX) and b) high density polyethylene (HDPE)[56]

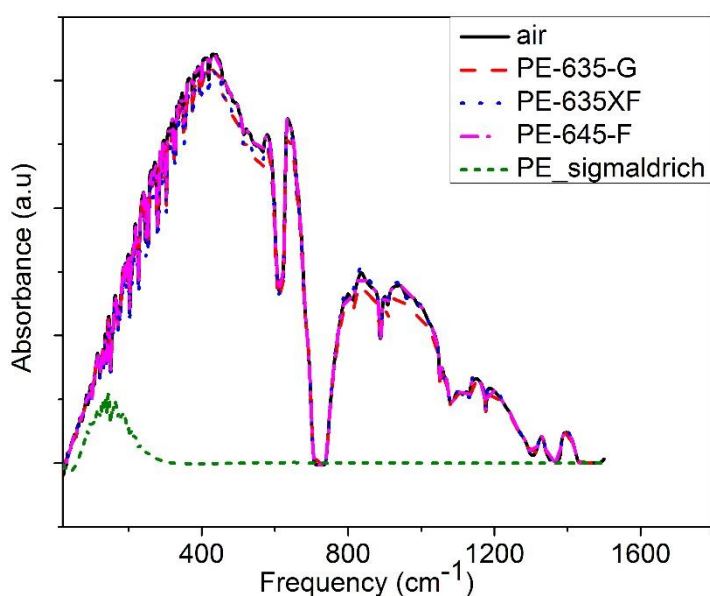


**Figure 43.** Comparison of different type of PE in terms of transmission properties

High density polyethylene is used as binder and diluent for pellet samples in THz region since it is highly transparent. The small grain size eases the pellet making process. There were 4 types of PE with different brands and/or sizes. Prior to measuring the API samples, it would be advantageous to determine the most transparent one. 635-G, 635-XF and 645-F PE samples were obtained from Micro Powder Incorporation's while one is obtained from Sigma-Aldrich. **Figure 43**

compares the Far-IR single beam spectra of these four different types of PE samples. The results showed that transparency of the Sigma-Aldrich one is very low compared to the others thus it is not considered for this study. Among the other three, 635-F type has the highest transparency in far-IR region of electromagnetic spectrum, thus, throughout this study it was chosen as the optimum binder and filler material for the pellets.

#### 4.1 THz Spectrum of Water Vapour

After the optimisation studies, the most abundant sample, water vapour, was decided to be collected. However, here the aim was neither to bring a new approach to the analysis nor to analyse in a wider bandwidth. The aim was rather to see the ability of observing the absorption features of the water and compare with the one reported in the literature. For this purpose, reference and sample spectra were measured in the presence and absence of purged air in the system. The resulting spectrum was presented in **Figure 44**. The spectrum shows that the water vapour has strong absorption features in THz region, all of which are well resolved and intense. Resonant absorption peaks are present at 1.16 THz, 1.70 THz, 2.23 THz and 2.75 THz in 0.1-3.0 THz frequency range. The observed bands are consistent with the literature.[57]

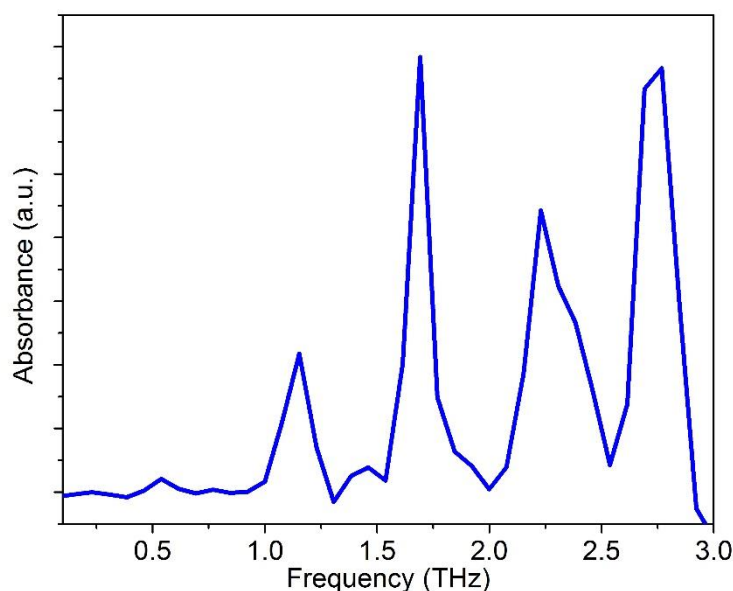


**Figure 44.** Absorption spectrum of water vapour

When compared with the literature study, the resolution seems rather low in the spectrum obtained. This is mostly related to the THz detection technique employed in this study. The electrooptic crystal used for detection of THz radiation causes multi reflection of THz pulse from air-crystal and crystal-air interfaces. These reflections affect the bandwidth of the spectrum during data analysis and results in narrower bandwidth. Good resolution is directly related to the time window scanned and since the window is limited by the multi-reflection of THz pulse, the resolution obtained was forced to be low.

## 4.2 THz spectra of APIs

### a. Meloxicam

Meloxicam is a nonsteroidal anti-inflammatory drug. Its working principle is to reduce the hormones that cause inflammation and pain in the body. Thus it is used for treating rheumatoid arthritis and osteoarthritis in adults.[58]

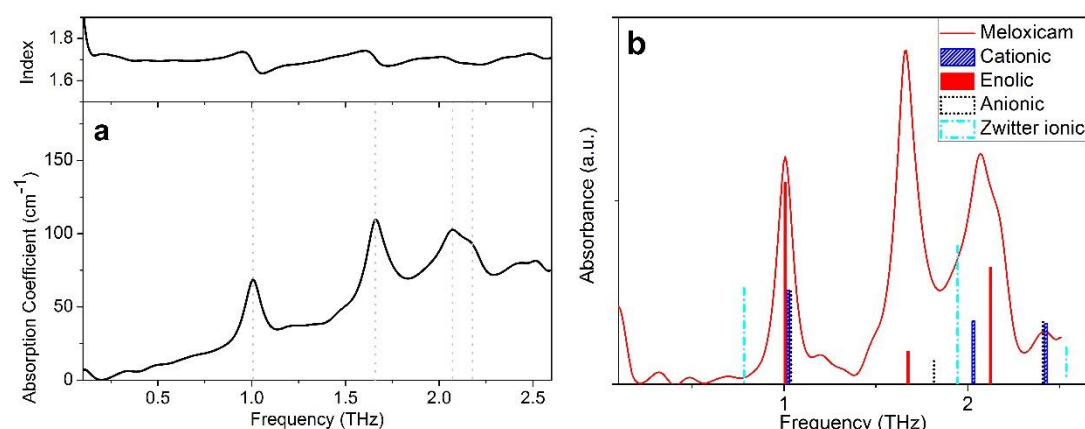


**Figure 45.** a) Frequency dependent absorption coefficient and refractive index of pure Meloxicam. b) Simulated spectra of enol (red) and cationic (blue) forms overlaying under the baseline corrected meloxicam spectrum.

In this part of the study we present optical properties of Meloxicam in the frequency range of 0.2 to 20 THz. **Figure 45a** shows frequency dependent THz absorption coefficient and refractive index of pure meloxicam in the range of 0.2-2.7 THz.

Meloxicam has well separated, prominent absorption bands located at 1.00, 1.66, 2.07 THz, and a broad, weak band at ca. 2.45 THz at room temperature. Especially the sharp band at 1.00 THz is a well resolved one and in a region where our TDS system has the highest SNR thus it can be used on identification and quantification of the drug. Such a strong and well separated features of Meloxicam will also be helpful in characterization of commercial ones when the technology advances. Due to strong attenuation and lower signal to noise ratio, it was not possible to obtain the spectrum of pure meloxicam with FT-THz. On the other hand, the frequency dependent index of Meloxicam in terahertz region is fairly linear with an average index of 1.68. The sudden changes on the refractive index are related with the strong absorptions observed in the pure meloxicam at those frequencies. The refractive index of the meloxicam is in the expected range of similar drugs.[39]

With experimental data alone it is not possible to identify the origin of the band as being intra or intermolecular vibrations, and theoretical calculations are a great help on the assignments in general. Meloxicam has four different polymorphs; anionic, cationic, zwitter-ionic and enolic forms.[59] Therefore, theoretical investigations should also consider all these four forms. The simulated stick spectra of these four forms are presented in **Figure 45b** together with a baseline corrected experimental meloxicam spectrum. The Figure clearly shows that the spectral features of each polymorph are very different from each other. Within the four simulated spectra enolic form (the preferred structure) of meloxicam have quite strong resembles to the experimental one, which could indicate the sample is mainly in its enolic form. The common peaks for the mentioned spectra are located at around 1.00, 1.67, and 2.12 THz. Intensity of the band observed at 1.66 THz in experimental spectrum is not proportional to the simulated spectrum. However, this could be due to two different reasons. The results of the calculations may not correctly simulate the relative intensities or the band is corresponding to a phonon mode that coincides with the simulated one. Considering that this band has strongest intensity in the experimental spectrum, second option is more likely. Thus, it is most probably a phonon mode rather than a molecular one. The simulated spectrum of cationic form also has features similar to the enolic form at 1.03, 2.04, and 2.43 THz. The broader feature centered at 2.07

THz in the experimental spectrum appears to be a combination of two modes. This and the broad mode at ca. 2.45 THz are best simulated when the spectral features of cationic form are considered together with enolic form in ca. 1:4 ratios. The bands of other modes do not seem to appear in the experimental spectrum.

**Figure 46a** shows the THz spectrum of Meloxicam at various amount in PE matrix. The vibrational features at 1.00 THz, 1.66 THz and 2.07 THz of meloxicam is clearly seen at every sample. Such a good agreement with the pure meloxicam shows that PE matrix has no or very small effect on the spectral features. However, the shoulder at 2.45 THz could not be observed possibly due to the loss of bandwidth with the addition of PE. **Figure 46b** presents the FT-THz spectra of 5% (w/w) meloxicam in PE measured with FT-THz spectrometer in a range of 1.5-20 THz. The spectrum is very rich as expected and has very strong features in this range. The FT-THz spectra is also presented **Figure 46a** as green line and the same bands are present at 1.66 THz and 2.07 THz within the common frequency range. The broad feature at 2.45 THz (not shown) confirms the existence of the shoulder observed in the THz spectrum of pure Meloxicam. The SNR of the FT-THz instrument is fairly low in this range and makes it very hard to identify the bands with FT-THz alone. Thus the help from the THz instrument is clearly needed for differentiating the bands in this low frequency region where THz technique is more powerful. Both techniques appear to be complementary to each other to obtain a wide spectrum and learn spectroscopic characteristics of the meloxicam.

THz-TDS spectra of the meloxicam in PE matrix with its well resolved bands presents itself as a possibility to do quantitative measures. Especially the band at 1.00 THz is very isolated and relatively higher in intensity and can be used for quantification of meloxicam. The band intensity at 1.00 THz correlates well with the meloxicam amount in PE matrix once it is corrected for scattering effect or simply after a base line correction. In addition, spectral comparison of the pure and in the matrix enabled to investigate the processing effect, mainly the applied pressure and stress on the structure. The pure meloxicam pellet was made under pressure of ca. 10 tons for 5 mins and application of such high pressure may affect the organization or may result

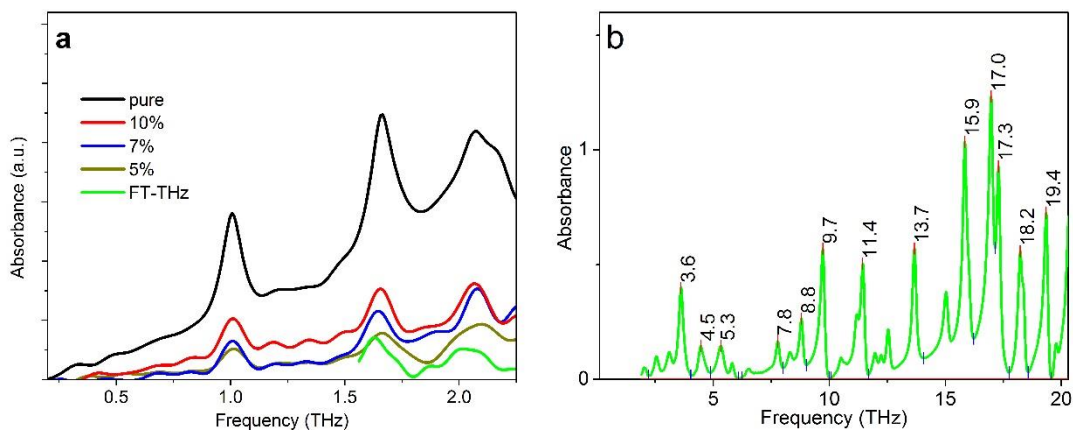


**Figure 46.** a) THz spectra of pure, 5 %, 7 %, and 10 % (w/w) Meloxicam in PE. The spectra of mixture samples were multiplied by 3 for clarity b) FT-THz spectrum of 5 % meloxicam over the range of 1.5 to 20 THz.

in structural changes. However, the meloxicam in PE was prepared with a pressure of only 1 ton. There is no significant difference between the pure and the matrix cases thus application of high pressure does not appear to have an observable effect on Meloxicam form.

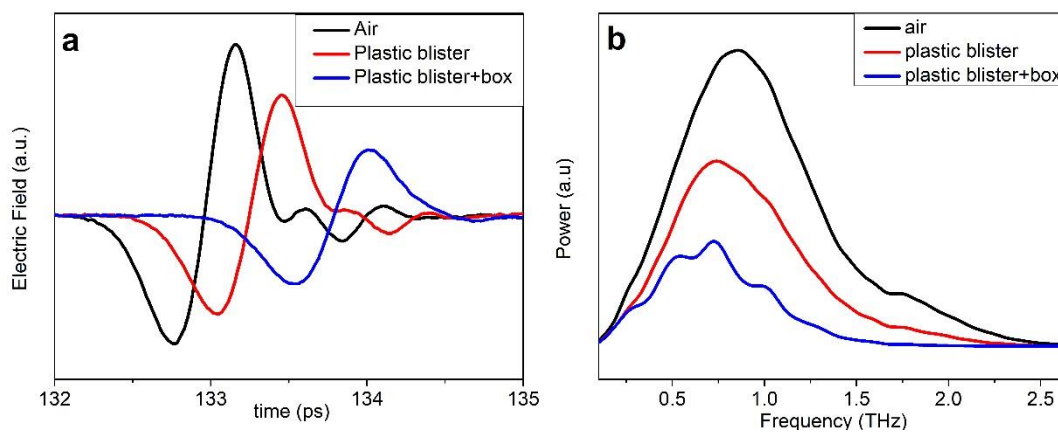


**Figure 47.** THz transmission study of drug host materials (box, plastic blister) a) time domain b) frequency domain data.

THz transparency of the packaging material used in the commercial drug Melox has been examined for the feasibility of drug measurements while the drug is in its package. **Figure 47** demonstrates the time domain THz field profile of various parts of the package (plastic blister, aluminum lid of the blister, the whole box except aluminum lid) and their corresponding frequency domain spectra. Even though the packaging material significantly attenuates the THz light, up to 1.5 THz appears to be enough for the API measurements in the tablet. The THz transmission is decreased ca.30 % with the plastic blister of the tablet. Then, it is decreased approximately another 30 % when cover box (secondary packing) is added. The results clearly show that THz beam has ability to reach the drug tablet by penetrating through paper cover and plastic enclosing. The aluminum foil used to protect and hold the drug in its cavity does not transmit the THz light but it is a good reflector, thus would enable collection of a spectrum in reflectance mode.

## b. Ibuprofen

Ibuprofen is one of the most commonly used nonsteroidal anti-inflammatory drug. It works by decreasing the level of hormones accounting for inflammation and pain resulted in situations like headache, toothache, back pain, arthritis, menstrual cramps, or minor injury.[60] The optical properties of 5 % and 10 % (w/w) Ibuprofen have been characterised by THz-TDS and FT-THz. (**Figure 48**) The 5 % sample spectrum had some hints for the location of the bands; however, the features' SNR is too low to describe as bands. Therefore, the concentration is increased to 10 %. With an increase in sensitivity of our instrument, detection of ibuprofen at lower concentrations would be possible.

As presented in **Figure 48a**, there are prominent absorption features for ibuprofen in THz region. The first peak located at  $36\text{ cm}^{-1}$  is quite intense and well resolved, on the other hand a less intense peak is at  $64\text{ cm}^{-1}$ . A possible shoulder is present at  $85\text{ cm}^{-1}$  with rather low in intensity and somehow is like hidden in the background caused by scattering of light, which increases with increasing frequency.

On the other hand, it has many distinguishable, well resolved absorption bands in its FT-THz spectrum located in the range of  $50\text{-}700\text{ cm}^{-1}$  that could also serve as fingerprints of the molecule. The main features are located at  $522\text{ cm}^{-1}$ ,  $589\text{ cm}^{-1}$  and  $667\text{ cm}^{-1}$ . The features present in THz and far-IR regions make it possible to analyse Ibuprofen both qualitatively and quantitatively.

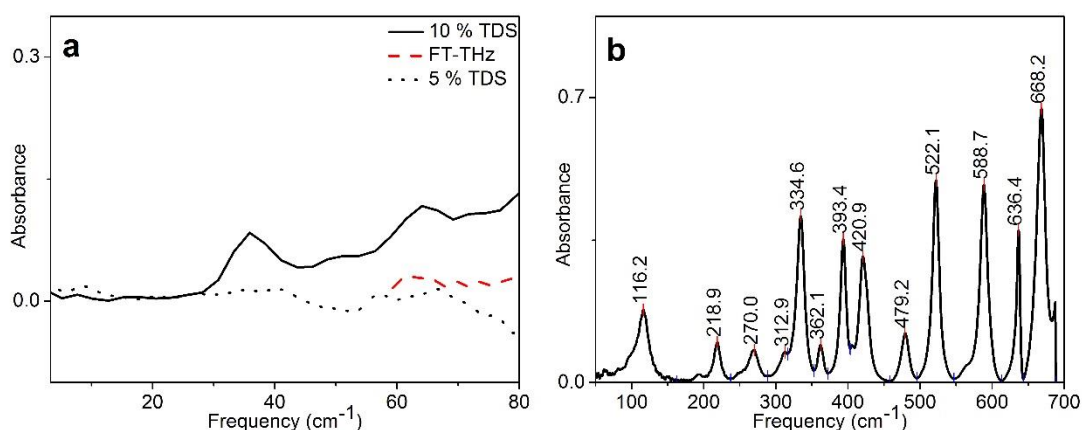


**Figure 48.** Spectra of 10 % and 5 % (w/w) Ibuprofen sample obtained by a) THz-TDS with samples (10 % and 5 % w/w) and b) FT-THz (5 % w/w) techniques

### c. Benzocaine

Benzocaine is a drug used for relieving pain and treating ear infections. It may also be used as local anesthetic. It reduces pain and discomfort in the ear.[61]

Optical properties of 2 % (w/w) benzocaine has been characterised by THz-TDS and FT-THz. Relatively strong but broad absorption bands of the molecule are observed at  $71\text{ cm}^{-1}$  and  $90\text{ cm}^{-1}$  in THz-TDS spectrum. (**Figure 49**) The peaks are resolved and their intensities are fairly good which could be utilised for quantitative purposes. On the other hand, the spectrum obtained by FT-THz technique resulted in prominent peaks in  $50\text{-}600\text{ cm}^{-1}$  frequency region (**Figure 49b**). The eminent absorption features could be very helpful for both qualitative and quantitative analysis of the molecule.

There are common spectral features for the spectra obtained by both systems. The peaks observed for TDS system are also observed at the same locations at the spectra collected by FT-THz system with lower SNR. The lower SNR can be attributed to the radiation source of FT-THz. This superposition of peaks in spectra obtained by two techniques would mean that these two techniques are complementary to each other resulting in enrichment of spectral information of Benzocaine. Also, the results showed that THz technique is a powerful technique that can be used for identification and characterisation of benzocaine.

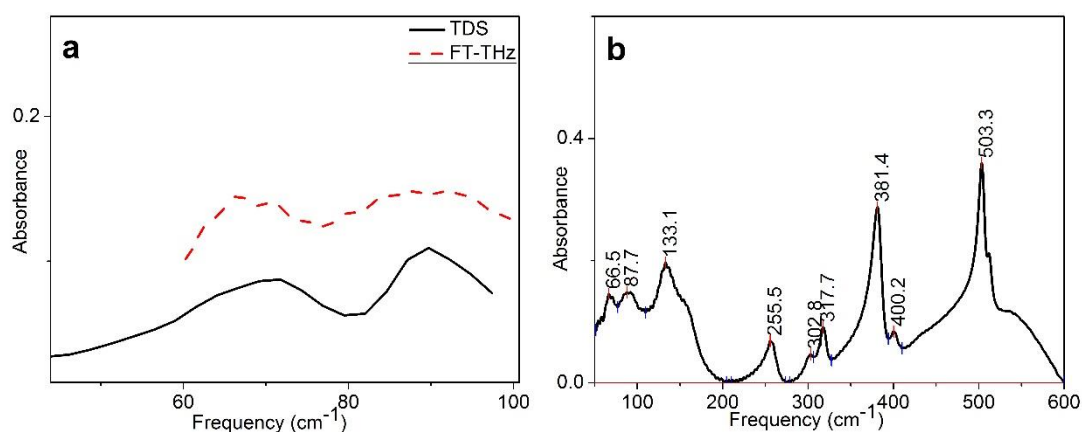


**Figure 49.** Spectra of 5 % w/w Benzocaine sample obtained by a) THz-TDS) and b) by FT-THz.

#### d. Fluoxetine HCl

Fluoxetine is an antidepressant used to treat major depressive disorder, bulimia nervosa (an eating disorder) obsessive-compulsive disorder, panic disorder, and premenstrual dysphoric disorder.[62]

The sample of Fluoxetine HCl has higher (10 %) concentration compared to the most of the other samples measured during this study which are usually around 5 %. The molecule has weak but observable resonant absorption features located at  $43\text{ cm}^{-1}$ ,  $69\text{ cm}^{-1}$  and  $85\text{ cm}^{-1}$  in the THz-TDS spectrum presented in **Figure 50a**. This spectral features are rather broad, possibly due to limited resolution. However, their intensities and resolution could be improved by having more concentrated sample of pure Fluoxetine as far as the SNR allows.

The FT-THz spectrum of Fluoxetine sample, on the other hand, possesses a common peak with THz spectrum and sharp, noticeable and well resolved absorption peaks at various intensities in a range of  $50\text{-}700\text{ cm}^{-1}$ . The main features are located at  $189\text{ cm}^{-1}$ ,  $636\text{ cm}^{-1}$  and  $648\text{ cm}^{-1}$ . Both THz and FT-THz features can be utilised to detect and discriminate Fluoxetine HCl in a fast and reliable way.

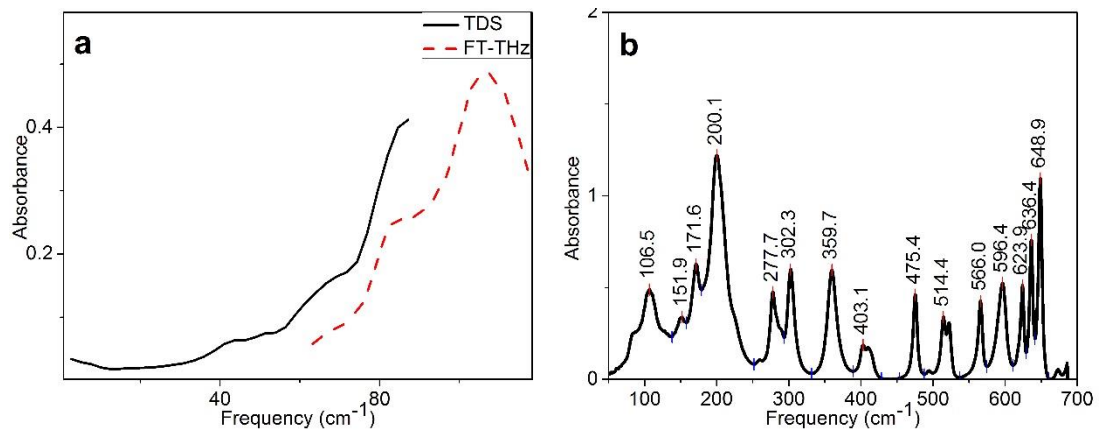


**Figure 50.** Spectra of Fluoxetine HCl sample obtained by a) THz-TDS (10 % w/w) and b) FT-THz (5 % w/w)

### e. Irbesartan

Irbesartan has property of preventing vessels from narrowing, which in turn decreases blood pressure and improves blood flow. Thus it is used for treatment of high blood pressure (hypertension). It is also used for curing kidney problems caused by type 2 diabetes.[63] The optical properties of 5 % (w/w) Irbesartan have been characterised by THz-TDS and FT-THz.(**Figure 51**)

The THz spectrum of Irbesartan sample showed distinct spectral features in 0.2-3 THz region. These features are located at  $33\text{ cm}^{-1}$  and  $49\text{ cm}^{-1}$ . The bands are slightly broader than usual but can serve as fingerprints of the molecule. They are low in intensity which is related to LOD for Irbesartan sample. FT-THz spectrum; however, is richer in terms of fingerprints since the technique works in wider frequency range. There are common bands with THz-TDS spectrum. The observed common features are most likely noise rather than absorption bands due to the low SNR of the instrument in this range. The main features of Irbesartan in far IR region are located at  $522\text{ cm}^{-1}$ ,  $625\text{ cm}^{-1}$  and  $665\text{ cm}^{-1}$ . Those discernible features, especially the ones below  $100\text{ cm}^{-1}$  are important for qualitative and quantitative analysis of the molecule.

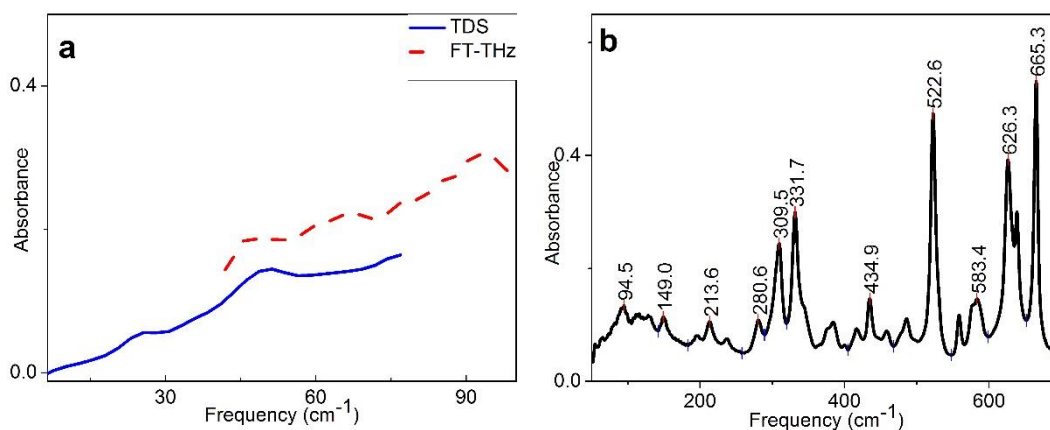


**Figure 51.** Spectra of 5 % (w/w) Irbesartan sample obtained by a) THz-TDS) and b) by FT-THz

## f. Losartan Potassium

Losartan potassium is also an API that prevents the blood vessels from narrowing, that in turn decreases blood pressure and develops blood flow. Therefore, the drug is used for treatment of high blood pressure (hypertension). Also, another usage of the drug is for lowering the risk of stroke in people with heart diseases.[64] The optical properties of 2 % and 5 % (w/w) Losartan Potassium have been characterised by THz-TDS and FT-THz. THz-TDS spectrum of the API showed noticeable absorption bands present at  $38\text{ cm}^{-1}$ ,  $70\text{ cm}^{-1}$  and  $94\text{ cm}^{-1}$ . (**Figure 52a**) The fact that the band located at  $70\text{ cm}^{-1}$  increases in intensity with the increase in concentration showing that the signal is analytical and quantitative measurements can be performed using the band at  $70\text{ cm}^{-1}$ . A feature lying around  $94\text{ cm}^{-1}$  became more discernible at 5 %; however, the bandwidth is not enough to fully resolve the feature. On the other hand, the band at  $38\text{ cm}^{-1}$  is only observable at 5 % sample as a weak and broad feature. With an increase in instrument sensitivity this feature can easily be identified even at lower concentrations and can also be used for quantification. On the other hand, FT-THz spectrum has many resonant absorption peaks in far IR region. (**Figure 52b**) Two of the bands located at  $70\text{ cm}^{-1}$  and  $94\text{ cm}^{-1}$  are within the common region, below  $100\text{ cm}^{-1}$ . The main features observed in the spectrum given in the **Figure 52b** are located at  $446\text{ cm}^{-1}$ ,  $539\text{ cm}^{-1}$  and  $565\text{ cm}^{-1}$ . Especially the bands lying at lower frequencies can be utilised for identification of Losartan potassium molecule.

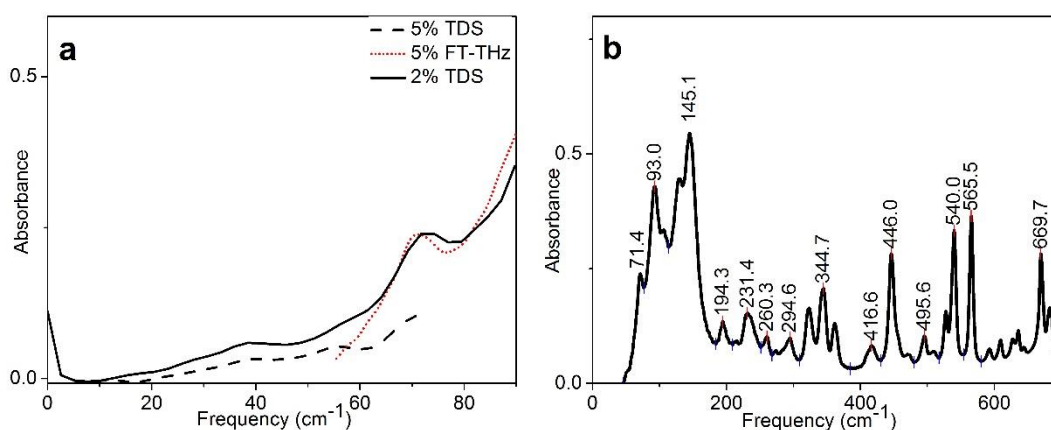


**Figure 52.** Spectra of 2 % and 5 % (w/w) Losartan Potassium sample obtained by a) THz-TDS (2 % and 5 % w/w) b) FT-THz (5 % w/w)

### g. Paracetamol

Paracetamol (acetaminophen) is a pain reliever and a fever reducer. Paracetamol is used for treatment of situations like headache, muscle aches, arthritis, backache, toothaches, colds, and fevers.[65] The optical properties of 2% and 5 % (w/w) Paracetamol have been characterised by THz-TDS and FT-THz. The THz-TDS spectra had spectral features located at 49  $\text{cm}^{-1}$ , 68  $\text{cm}^{-1}$  and 94  $\text{cm}^{-1}$ . (**Figure 53a**) The study showed that the features increased both in intensity and resolution with increasing concentration. The peaks located at 49  $\text{cm}^{-1}$  and 94  $\text{cm}^{-1}$  became more observable at 5% w/w.

FT-THz spectrum of the molecule, on the other hand, has many novel absorption peaks that lie between 60  $\text{cm}^{-1}$ -700  $\text{cm}^{-1}$ . (**Figure 53b**) It should be noted that THz-TDS and FT-THz spectra have common modes located at 68  $\text{cm}^{-1}$  and 94  $\text{cm}^{-1}$ . Those novel characteristic peaks of Paracetamol have good resolution and high intensities. The main bands of the molecule are located at 215  $\text{cm}^{-1}$ , 338  $\text{cm}^{-1}$ , 503  $\text{cm}^{-1}$  and 517  $\text{cm}^{-1}$ .

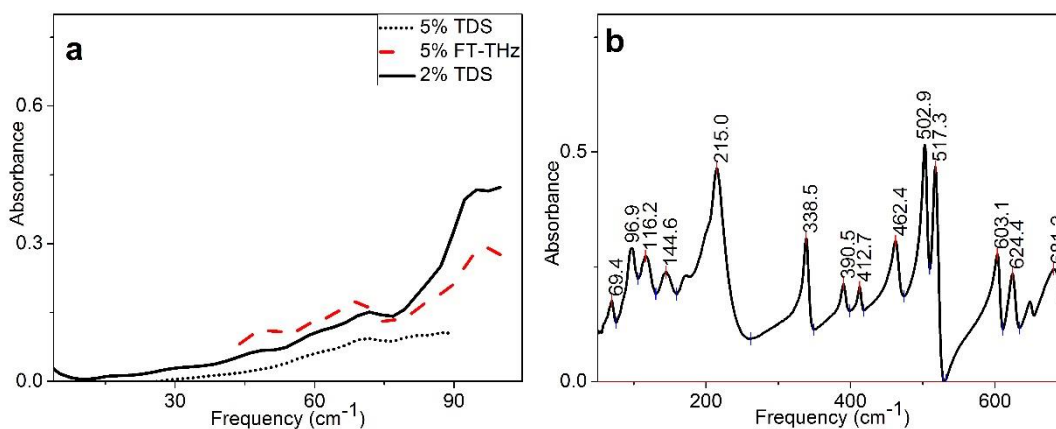


**Figure 53.** Spectra of Paracetamol sample obtained by a) THz-TDS (2 and 5 % w/w) b) FT-THz (5 % w/w).

## h. Ranitidine HCl

Ranitidine HCl is an API used in drugs for treating and preventing ulcers in the stomach and intestines by reducing the amount of acid produced by the stomach.[66] The optical properties of 5 % (w/w) Irbesartan have been characterised by THz-TDS and FT-THz. As presented in **Figure 54a**, the molecule possesses bands in its THz spectrum that are located at  $41\text{ cm}^{-1}$ ,  $67\text{ cm}^{-1}$ , and  $82\text{ cm}^{-1}$ . The features are broad in nature due to low absorption of the molecule. There were two samples of Ranitidine HCl with concentrations of 2% and 5% w/w. The peak observed at  $41\text{ cm}^{-1}$  increased in intensity as the concentration increased, which shows it could be used for quantitative purposes. Other two peaks observed in 2% did not show significant change in intensity when concentration was increased to 5%. However, it was observed that as the concentration increased the slope of the background in the spectrum increased indicating an increase in scattering

The molecule also has a rich FT-THz spectrum with many prominent absorption features that could be used for identification of the molecule. (**Figure 54b**) There are common absorption peaks in the spectra obtained by the two techniques used to measure the sample. The shoulder at  $82\text{ cm}^{-1}$  present in THz spectrum is also shared by the FT-THz spectrum. Thus when the two techniques are combined it can be quite helpful for quantitative and qualitative analysis of Ranitidine HCl in a quite wide frequency range. The main bands of the molecule are located at  $149\text{ cm}^{-1}$ ,  $189\text{ cm}^{-1}$  and  $523\text{ cm}^{-1}$  in the far IR spectrum.

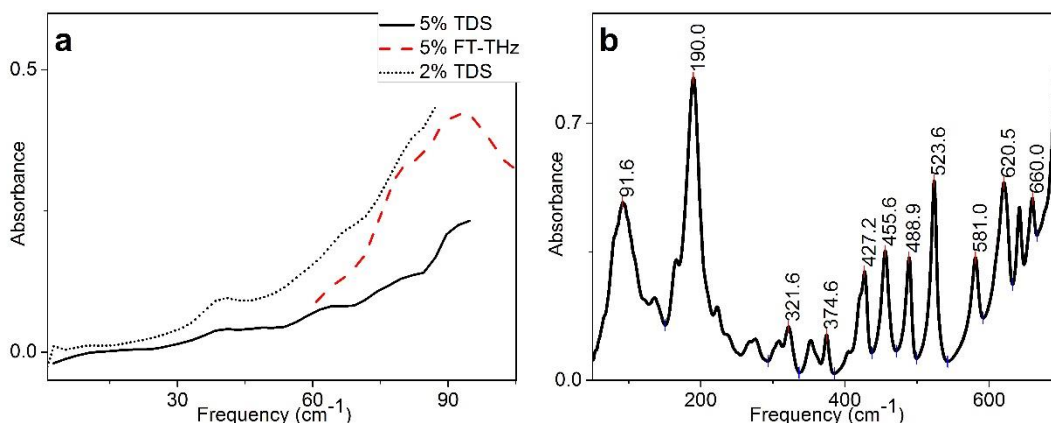


**Figure 54.** Spectra of 2 and 5 % (w/w) Ranitidine HCl sample obtained by a) THz-TDS (2 and 5 % w/w) and b) FT-THz (2 % w/w)

### i. Cinnarizine

The API Cinnarizine is helpful to problems present in inner ear and balance, like dizziness and sickness. It could also be used for treating travel sickness.[67] Optical properties of 5 % (w/w) Cinnarizine has been characterised by THz-TDS and FT-THz. Terahertz spectrum of the molecule is shown in **Figure 55a**. The sample of Cinnarizine did not show any spectral features in THz region. One reason could be that the sample concentration is below the limit of detection (LOD) of the system thus it could not be sensed. However, there is no sign for any absorption band below  $100\text{ cm}^{-1}$  on FT-THz spectrum, either. (**Figure 55b**).

FT-THz spectra of the Cinnarizine sample is shown in **Figure 55b**. The spectra showed prominent resonant absorption bands present in far-IR region. The peaks are well resolved and so intense that they could be used for determination of Cinnarizine. The most intense features are located at  $379\text{ cm}^{-1}$ ,  $471\text{ cm}^{-1}$ ,  $566\text{ cm}^{-1}$  and  $629\text{ cm}^{-1}$ .

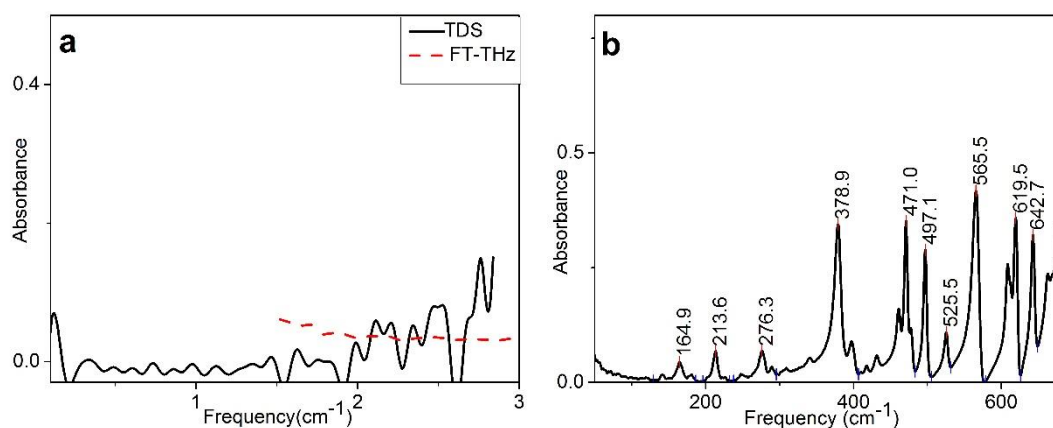


**Figure 55.** Spectra of 5 % (w/w) Cinnarizine sample obtained by a) THz-TDS) and b) FT-THz.

### j. Desloratadine

Desloratadine is an antihistaminic API used against the effects of the naturally abundant chemical in body, histamine. Thus, it is used for treating the symptoms of allergies, like sneezing, watery eyes, and runny nose. It is also used to treat skin hives and itching in people with chronic skin reactions.[68] Optical properties of 5 % (w/w) Desloratadine has been characterised by THz-TDS and FT-THz. In THz region the Desloratadine sample has a featureless spectrum as presented in **Figure 56a**, which is confirmed by the far-IR spectrum.

On the other hand, the FT-THz spectrum of Desloratadine contains characteristic peaks for the molecule, that are well resolved and intense. (**Figure 56b**) The peak intensities increase gradually in the spectrum as the frequency increases. Such rich features can be utilised for identification and quantification of the drug on the market. The main features are located at  $448\text{ cm}^{-1}$ ,  $488\text{ cm}^{-1}$ ,  $529\text{ cm}^{-1}$  and  $569\text{ cm}^{-1}$ .

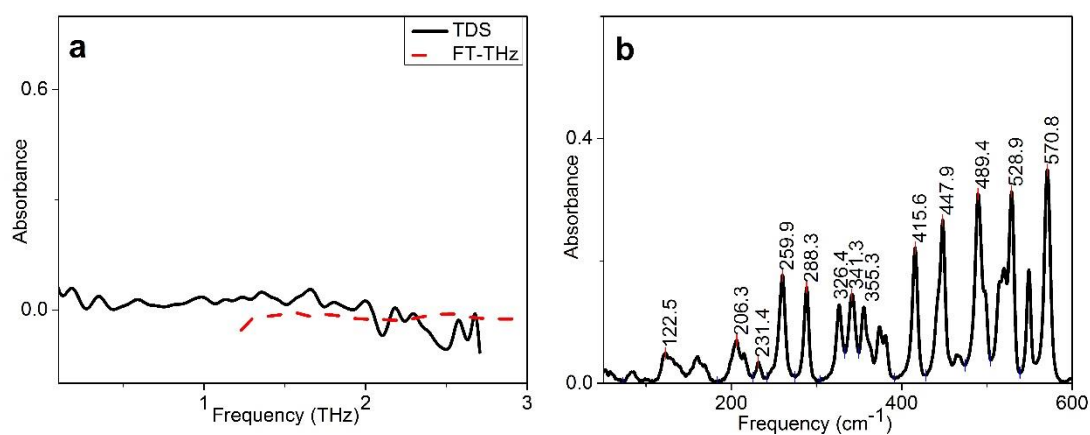


**Figure 56.** Spectra of 5% (w/w) Desloratadine sample obtained by a) THz-TDS) and b) FT-THz

### k. Telmisartan

Telmisartan is an API used in drugs that is for treating high blood pressure (hypertension). It keeps blood vessels from narrowing, as a result it lowers blood pressure and improves blood flow.[69] The optical properties of 5 % (w/w) Telmisartan have been characterised by THz-TDS and FT-THz. THz spectrum of the Telmisartan molecule is shown in **Figure 57a**. The molecule has a featureless spectrum in THz region. A more concentrated sample could be investigated to be sure about whether the molecule shows characteristic peaks in THz region.

FT-THz spectrum of the molecule has noticeable absorption peaks in far IR region as presented in **Figure 57b**. There are intense and well resolved bands in the spectrum that are useful for quantitative purposes. The main features are located at  $542\text{ cm}^{-1}$ ,  $574\text{ cm}^{-1}$  and  $668\text{ cm}^{-1}$ .

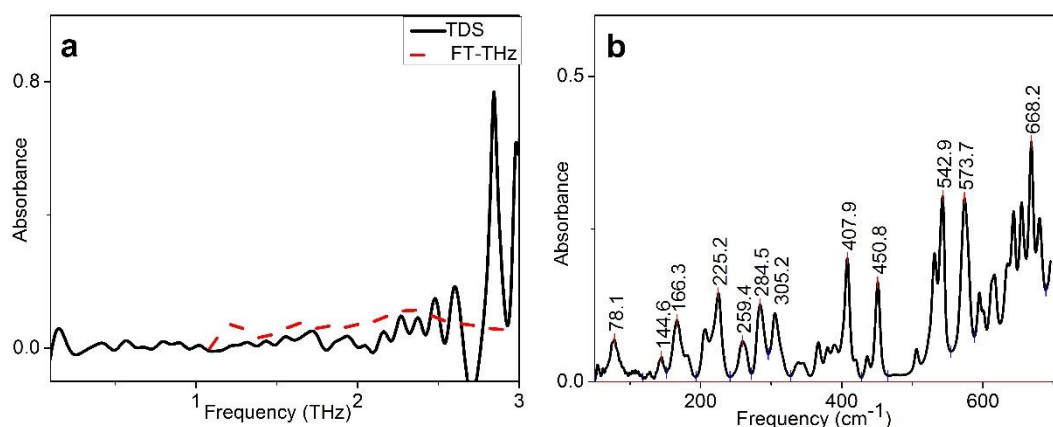


**Figure 57.** Spectra of 5 % (w/w) Telmisartan sample obtained by a) THz-TDS and b) FT-THz

## CHAPTER 5

### CONCLUSION

In this study we aimed to build a THz-TDS spectrometer, optimise the system and finally show its successful use in optical characterisation of Benzocaine, Cinnarizine, Desloratadine, Fluoxetine HCl, Ibuprofen, Irbesartan, Losartan Potassium, Meloxicam, Paracetamol, Ranitidine HCl, and Telmisartan samples. For application purpose, we have chosen characterisation of active pharmaceutical ingredients since THz spectroscopy gains significant attention in this field with its unique properties. During the spectrometer set-up process various optical designs were considered that utilise various antenna-antenna combinations or antenna-crystal combinations.

At first antenna-antenna combinations were tried as generation and detection of THz field due to its easiness to set-up and previously described advantages. Although initial set-ups of PCA for generation and iPCA for detection or iPCA for generation and PCA for detection were successful, the recorded THz field and profile had very low SNR and very limited DR in both cases. Later THz generation with an antenna and its detection with electro-optic sampling were tried. In this case, the use of PCA for generation and 0.5 mm <110> ZnTe for detection also yielded low SNR. However, the combination set-up of iPCA antenna and ZnTe crystal for generation and detection of THz light had yield the best SNR and widest DR both in time and frequency domains. Therefore, all the optimisation procedures were carried out on this set-up.

Various processes were followed during optimisation of the system. One of the main problem was the Teflon lens used in the antenna assembly. After the removal of Teflon lens in front of the antenna, the SNR significantly increased. The stage settings were also important for having an optimum system. The scanning mode were chosen to be

continuous mode because it takes far less time and provides good SNR as compared to step scanning mode. The lock-in parameters like time constant, sensitivity, signal input settings, and reserve settings were also optimised. The first two settings had significant effect on the signal. On the other hand, the last three settings had very minimum contribution to SNR. Eliminating the water vapour from the system also improved the signal. The bandwidth expanded to ca. 3 THz, the high frequency signal increased further by removal of water bands from the THz spectra.

The optimisations studies were followed an application study of API characterisations. The THz spectra of APIs showed that the THz-TDS technique provides new and unique information about the molecules. This information obtained can be very useful for identification and quantification of API molecules. When combined with the unique properties of THz technique that are being non-invasive, non-destructive and non-ionising, in-line and on-line analysis of drugs may become possible. Therefore, in near future fast and reliable analysis of API molecules would be possible with further advances in the THz technology.

## REFERENCES

- [1] D. Dragoman and M. Dragoman, "Terahertz fields and applications," *Prog. Quantum Electron.*, vol. 28, no. 1, pp. 1–66, 2004.
- [2] S. Dexheimer, Ed., "Terahertz Spectroscopy: Principles and Applications," in *Terahertz Spectroscopy: Principles and Applications*, Taylor & Francis, 2007, p. 360.
- [3] P. R. Smith, D. H. Auston, and M. C. Nuss, "Subpicosecond Photoconducting Dipole Antennas," *IEEE J. Quantum Electron.*, vol. 24, no. 2, pp. 255–260, 1988.
- [4] C. Fattinger and D. Grischkowsky, "Terahertz beams," *Appl. Phys. Lett.*, vol. 54, no. 6, pp. 490–492, 1989.
- [5] M. D. King, W. D. Buchanan, and T. M. Korter, "Understanding the Terahertz Spectra of Crystalline Pharmaceuticals: Terahertz Spectroscopy and Solid-State Density Functional Theory Study of (S)-(+)-Ibuprofen and (RS)-Ibuprofen," *J. Pharm. Sci.*, vol. 100, no. 3, pp. 1116–1129, 2011.
- [6] D. F. Plusquellic, K. Siegrist, E. J. Heilweil, and O. Esenturk, "Applications of terahertz spectroscopy in biosystems," *ChemPhysChem*, vol. 8, no. 17, pp. 2412–2431, 2007.
- [7] O. Esenturk, J. S. Melinger, P. A. Lane, and E. J. Heilweil, "Ultrafast Photoinduced Carrier Dynamics of Organic Semiconductors Measured by Time-resolved Terahertz Spectroscopy," *Org. Thin Film. Photonic Appl.*, vol. 1039, pp. 241–254, 2010.
- [8] O. Esenturk, J. S. Melinger, and E. J. Heilweil, "Photoconductivity of organic semiconductor polymers studied by time-resolved THz-TDS," *2007 Jt. 32Nd Int. Conf. Infrared Millim. Waves 15Th Int. Conf. Terahertz Electron. Vols 1*

- 2, pp. 655–656, 2007.
- [9] C. J. Docherty and M. B. Johnston, “Terahertz properties of graphene,” *J. Infrared, Millimeter, Terahertz Waves*, vol. 33, no. 8, pp. 797–815, 2012.
- [10] M. C. Kemp, P. F. Taday, B. E. Cole, J. Cluff, A. J. Fitzgerald, and W. R. Tribe, “Security applications of terahertz technology,” *Proc. SPIE*, vol. 5070, pp. 44–52, 2003.
- [11] F. Fan, W. Li, W. H. Gu, X. H. Wang, and S. J. Chang, “Cross-shaped metal-semiconductor-metal plasmonic crystal for terahertz modulator,” *Photonics Nanostructures - Fundam. Appl.*, vol. 11, no. 1, pp. 48–54, 2013.
- [12] M. He, A. K. Azad, S. Ye, and W. Zhang, “Far-infrared signature of animal tissues characterized by terahertz time-domain spectroscopy,” *Opt. Commun.*, vol. 259, no. 1, pp. 389–392, 2006.
- [13] Y. Jiang, F. Zhou, X. Wen, L. Yang, G. Zhao, H. Wang, H. Wang, Y. Zhai, J. Wu, K. Liu, and J. Chen, “Terahertz absorption spectroscopy of benzamide, acrylamide, caprolactam, salicylamide, and sulfanilamide in the solid state,” *J. Spectrosc.*, vol. 2014, pp. 1–9, 2014.
- [14] P. A. Lane, P. D. Cunningham, J. S. Melinger, O. Esenturk, and E. J. Heilweil, “Hot photocarrier dynamics in organic solar cells,” *Nat. Commun.*, vol. 6, p. 7558, 2015.
- [15] B. Ferguson and X.-C. Zhang, “Materials for terahertz science and technology,” *Nat. Mater.*, vol. 1, no. 1, pp. 26–33, 2002.
- [16] Y. C. Shen, P. C. Upadhyaya, E. H. Linfield, H. E. Beere, and A. G. Davies, “Ultrabroadband terahertz radiation from low-temperature-grown GaAs photoconductive emitters,” *Appl. Phys. Lett.*, vol. 83, no. 15, pp. 3117–3119, 2003.
- [17] A. Bonvalet, M. Joffre, J. L. Martin, and A. Migus, “Generation of ultrabroadband femtosecond pulses in the mid-infrared by optical rectification of 15 fs light pulses at 100 MHz repetition rate,” *Appl. Phys. Lett.*, vol. 67, no.

- 1995, p. 2907, 1995.
- [18] J. B. Baxter and G. W. Guglietta, "Terahertz Spectroscopy," *Anal. Chem.*, vol. 83, pp. 4342–4368, 2011.
- [19] E. Arik, H. Altan, and O. Esenturk, "Dielectric Properties of Diesel and Gasoline by Terahertz Spectroscopy," *J. Infrared, Millimeter, Terahertz Waves*, vol. 35, pp. 759–769, 2014.
- [20] P. A. Lane, P. D. Cunningham, J. S. Melinger, G. P. Kushto, O. Esenturk, and E. J. Heilweil, "Photoexcitation dynamics in films of C 60 and Zn phthalocyanine with a layered nanostructure," *Phys. Rev. Lett.*, vol. 108, no. 7, pp. 1–5, 2012.
- [21] O. Esenturk, A. Evans, and E. J. Heilweil, "Terahertz spectroscopy of dicyanobenzenes: Anomalous absorption intensities and spectral calculations," *Chem. Phys. Lett.*, vol. 442, no. 1–3, pp. 71–77, 2007.
- [22] G. C. Loata, M. D. Thomson, T. Löffler, and H. G. Roskos, "Radiation field screening in photoconductive antennae studied via pulsed terahertz emission spectroscopy," *Appl. Phys. Lett.*, vol. 91, no. 23, pp. 1–4, 2007.
- [23] U. Welp, K. Kadowaki, and R. Kleiner, "Superconducting emitters of THz radiation," *Nat. Photonics*, vol. 7, no. 9, pp. 702–710, 2013.
- [24] M. Kreß, T. Löffler, M. D. Thomson, R. Dörner, H. Gimpel, K. Zrost, T. Ergler, R. Moshhammer, U. Morgner, J. Ullrich, and H. G. Roskos, "Determination of the carrier-envelope phase of few-cycle laser pulses with terahertz-emission spectroscopy," *Nat. Phys.*, vol. 2, pp. 327–332, 2006.
- [25] S. P. Delaney and T. M. Korter, "Terahertz Spectroscopy and Computational Investigation of the Flufenamic Acid/Nicotinamide Cocrystal," *J. Phys. Chem. A*, vol. 119, no. 13, pp. 3269–3276, 2015.
- [26] M. Ge, G. Liu, S. Ma, and W. Wang, "Polymorphic forms of furosemide characterized by THz time domain spectroscopy," *Bull. Korean Chem. Soc.*, vol. 30, no. 10, pp. 2265–2268, 2009.

- [27] C. J. Strachan, P. F. Taday, D. a. Newnham, K. C. Gordon, J. A. Zeitler, M. Pepper, and T. Rades, "Using terahertz pulsed spectroscopy to quantify pharmaceutical polymorphism and crystallinity," *J. Pharm. Sci.*, vol. 94, no. 4, pp. 837–846, 2005.
- [28] C. J. Strachan, T. Rades, D. a. Newnham, K. C. Gordon, M. Pepper, and P. F. Taday, "Using terahertz pulsed spectroscopy to study crystallinity of pharmaceutical materials," *Chem. Phys. Lett.*, vol. 390, no. 1–3, pp. 20–24, 2004.
- [29] W. L. Chan, J. Deibel, and D. M. Mittleman, "Imaging with terahertz radiation," *Reports Prog. Phys.*, vol. 70, no. 8, pp. 1325–1379, 2007.
- [30] K. Fukunaga, I. Hosako, M. Picollo, and Y. Kohdzuma, "Application of THz sensing to analysis of works of art for conservation," *Proc. - 2010 IEEE Int. Top. Meet. Microw. Photonics, MWP 2010*, vol. 2, pp. 147–150, 2010.
- [31] M. D. King, W. D. Buchanan, and T. M. Korter, "Identification and quantification of polymorphism in the pharmaceutical compound diclofenac acid by terahertz spectroscopy and solid-state density functional theory," *Anal. Chem.*, vol. 83, no. 10, pp. 3786–3792, 2011.
- [32] P. F. Taday, I. V Bradley, D. D. Arnone, and M. Pepper, "Using terahertz pulse spectroscopy to study the crystalline structure of a drug: A case study of the polymorphs of ranitidine hydrochloride - Taday - 2003 - Journal of Pharmaceutical Sciences - Wiley Online Library," *J. Pharm. Sci.*, vol. 92, no. 4, pp. 831–838, 2003.
- [33] S. Byrn, R. Pfeiffer, M. Ganey, C. Hoiberg, and G. Poochikian, "Pharmaceutical Solids: A Strategic Approach to Regulatory Considerations," *Pharmaceutical Research: An Official Journal of the American Association of Pharmaceutical Scientists*, vol. 12, no. 7. pp. 945–954, 1995.
- [34] M. K. Riekes, R. N. Pereira, G. S. Rauber, S. L. Cuffini, C. E. M. de Campos, M. A. S. Silva, and H. K. Stulzer, "Polymorphism in nimodipine raw materials: Development and validation of a quantitative method through

- differential scanning calorimetry,” *J. Pharm. Biomed. Anal.*, vol. 70, pp. 188–193, 2012.
- [35] A. D. Patel, P. E. Luner, and M. S. Kemper, “Low-level determination of polymorph composition in physical mixtures by near-infrared reflectance spectroscopy,” *J. Pharm. Sci.*, vol. 90, no. 3, pp. 360–370, 2001.
- [36] J. Seliger, V. Žagar, T. Apih, A. Gregorovič, M. Latosińska, G. A. Olejniczak, and J. N. Latosińska, “Polymorphism and disorder in natural active ingredients. Low and high-temperature phases of anhydrous caffeine: Spectroscopic ( $^1\text{H}$ – $^{14}\text{N}$  NMR–NQR/ $^{14}\text{N}$  NQR) and solid-state computational modelling (DFT/QTAIM/RDS) study,” *Eur. J. Pharm. Sci.*, vol. 85, pp. 18–30, 2016.
- [37] Y. Xin, H. Y. Oderji, R. Hai, and H. Bin Ding, “Molecular Dynamics Simulation on Terahertz Spectra of Methamphetamine Hydrochloride,” *Adv. Mater. Res.*, vol. 760–762, pp. 35–39, 2013.
- [38] J. A. Zeitler, D. a. Newnham, P. F. Taday, C. J. Strachan, M. Pepper, K. C. Gordon, and T. Rades, “Temperature dependent terahertz pulsed spectroscopy of carbamazepine,” *Thermochim. Acta*, vol. 436, no. 1–2, pp. 71–77, 2005.
- [39] J. A. Zeitler, K. Kogermann, J. Rantanen, T. Rades, P. F. Taday, M. Pepper, J. Aaltonen, and C. J. Strachan, “Drug hydrate systems and dehydration processes studied by terahertz pulsed spectroscopy,” *Int. J. Pharm.*, vol. 334, no. 1–2, pp. 78–84, 2007.
- [40] L. Yang, H. Sun, S. Weng, K. Zhao, L. Zhang, G. Zhao, Y. Wang, Y. Xu, X. Lu, C. Zhang, J. Wu, and C. Jia’er, “Terahertz absorption spectra of some saccharides and their metal complexes,” *Spectrochim. Acta - Part A Mol. Biomol. Spectrosc.*, vol. 69, no. 1, pp. 160–166, 2008.
- [41] J. Sibik and J. A. Zeitler, “Direct measurement of molecular mobility and crystallisation of amorphous pharmaceuticals using terahertz spectroscopy,” *Adv. Drug Deliv. Rev.*, 2016.
- [42] J. Sibik, M. J. Sargent, M. Franklin, and J. A. Zeitler, “Crystallization and

- phase changes in paracetamol from the amorphous solid to the liquid phase,” *Mol. Pharm.*, vol. 11, no. 4, pp. 1326–1334, 2014.
- [43] J. Sibik and J. Axel Zeitler, “Direct measurement of molecular mobility and crystallisation of amorphous pharmaceuticals using terahertz spectroscopy,” *Adv. Drug Deliv. Rev.*, no. 2016, 2016.
- [44] J. Shen, G. Wang, D. Jiang, L. Liang, and X. Xu, “Terahertz spectroscopic investigations of caffeine and 3-acetylmorphine,” *Optik (Stuttg.)*, vol. 121, no. 18, pp. 1712–1716, 2010.
- [45] S. Jin-Hai, S. Jing-Ling, L. Lai-Shun, X. Xiao-Yu, L. Hai-Bo, Z. Cun-Lin, J. H. Sun, J. L. Shen, L. S. Liang, X. Y. Xu, H. B. Liu, and C. L. Zhang, “Experimental Investigation on Terahertz Spectra of Amphetamine Type Stimulants,” *Chinese Phys. Lett.*, vol. 22, no. 12, pp. 3176–3178, 2005.
- [46] P. Hakey, W. Ouellette, J. Zubieta, and T. Korter, “Redetermination of (+)-methamphetamine hydrochloride at 90 K,” *Acta Crystallogr. Sect. E Struct. Reports Online*, vol. 64, no. 5, pp. o940–o940, 2008.
- [47] A. Dobroiu, Y. Sasaki, T. Shibuya, C. Otani, and K. Kawase, “THz-wave spectroscopy applied to the detection of illicit drugs in mail,” *Proc. IEEE*, vol. 95, no. 8, pp. 1556–1575, 2007.
- [48] A. J. Fitzgerald, B. E. Cole, and P. F. Taday, “Nondestructive analysis of tablet coating thicknesses using Terahertz pulsed imaging,” *J. Pharm. Sci.*, vol. 94, no. 1, pp. 177–183, 2005.
- [49] BATOP, “Instruction manual and data sheet PCA-40-05-10-800-x.” [Online]. Available: [http://www.batop.com/products/terahertz/photoconductive-antenna/data-sheet/manual\\_PCA-40-05-10-800.pdf](http://www.batop.com/products/terahertz/photoconductive-antenna/data-sheet/manual_PCA-40-05-10-800.pdf). [Accessed: 07-Jul-2016].
- [50] BATOP, “Instruction manual and data sheet iPCA-21-05-1000-1040-h.” [Online]. Available: <http://www.batop.com/information/news/hpa.pdf>. [Accessed: 07-Jul-2016].
- [51] C. A. Schmuttenmaer, “Exploring dynamics in the far-infrared with terahertz

- spectroscopy,” *Chem. Rev.*, vol. 104, no. 4, pp. 1759–1779, 2004.
- [52] Stanford Research Systems, “MODEL SR830 DSP Lock-In Amplifier,” 2011. [Online]. Available: <http://www.thinksrs.com/downloads/PDFs/Manuals/SR830m.pdf>. [Accessed: 04-Apr-2016].
- [53] “Synchronous amplifier / benchtop / DSP SR810, SR830.” [Online]. Available: <http://www.directindustry.com/prod/stanford-research-systems/product-7218-54625.html>.
- [54] H. Hoshina, “TDS Spectrum Viewer.” Tokyo, 2011.
- [55] M. Naftaly and R. Dudley, “Methodologies for determining the dynamic ranges and signal-to-noise ratios of terahertz time-domain spectrometers.,” *Opt. Lett.*, vol. 34, no. 8, pp. 1213–1215, 2009.
- [56] TYDEX, “THz Materials.” [Online]. Available: [http://www.tydexoptics.com/products/thz\\_optics/thz\\_materials/](http://www.tydexoptics.com/products/thz_optics/thz_materials/). [Accessed: 07-Jul-2016].
- [57] W. Withayachumnankul, B. M. Fischer, and D. Abbott, “Numerical removal of water vapour effects from terahertz time-domain spectroscopy measurements,” *Proc. R. Soc. A*, vol. 464, no. October 2007, pp. 2435–2456, 2008.
- [58] C. Multum, “Meloxicam,” 2016. [Online]. Available: <https://www.drugs.com/cdi/meloxicam.html>. [Accessed: 07-Jul-2016].
- [59] W. Snor, E. Liedl, P. Weiss-Greiler, H. Viernstein, and P. Wolschann, “Density functional calculations on meloxicam- $\beta$ -cyclodextrin inclusion complexes,” *Int. J. Pharm.*, vol. 381, no. 2, pp. 146–152, 2009.
- [60] C. Multum, “Ibuprofen,” 2015. [Online]. Available: <https://www.drugs.com/ibuprofen.html>. [Accessed: 07-Jul-2016].
- [61] C. Multum, “Benzocaine topical.” [Online]. Available: <https://www.drugs.com/mtm/benzocaine-topical.html>. [Accessed: 07-Jul-

- 2016].
- [62] C. Multum, “Fluoxetine,” 2015. [Online]. Available: <https://www.drugs.com/fluoxetine.html>. [Accessed: 07-Jul-2016].
- [63] C. Multum, “Irbesartan,” 2014.
- [64] C. Multum, “Losartan.” [Online]. Available: <https://www.drugs.com/losartan.html>. [Accessed: 07-Jul-2016].
- [65] C. Multum, “Paracetamol,” 2009. [Online]. Available: <https://www.drugs.com/paracetamol.html>. [Accessed: 07-Jul-2016].
- [66] C. Multum, “Ranitidine,” 2010. [Online]. Available: <https://www.drugs.com/ranitidine.html>. [Accessed: 07-Jul-2016].
- [67] H. Allen, “Cinnarizine tablets (Stugeron),” 2015. [Online]. Available: <http://patient.info/medicine/cinnarizine-tablets-stugeron>. [Accessed: 07-Jul-2016].
- [68] C. Multum, “Desloratadine,” 2011. [Online]. Available: <https://www.drugs.com/mtm/desloratadine.html>. [Accessed: 07-Jul-2016].
- [69] C. Multum, “Telmisartan,” 2014. [Online]. Available: <https://www.drugs.com/mtm/telmisartan.html>. [Accessed: 07-Jul-2016].